NUMERICAL MODELING OF NEARSHORE WAVE TRANSFORMATION USING THE MESHLESS MULTIQUADRIC METHOD

by

Zeynep Adak

B.S., Industrial Engineering, Marmara University, 2007

Submitted to the Institute for Graduate Studies in
Science and Engineering in partial fulfillment of
the requirements for the degree of
Master of Science

Graduate Program in Computational Science and Engineering

Boğaziçi University

2011

ACKNOWLEDGEMENTS

I would like to express my greatest appreciation and gratitude to my supervisor Dr. Osman Börekçi for his support and guidance throughout the preparation of this thesis. I would also like to thank other committee members, Dr. K. Atalık and Dr. E. N. Otay, for their comments, suggestions and assistance.

My sincere appreciation is extended to Dr. Sadettin Ökten for his moral support and encouragement right through my graduate study.

Finally, special thanks go to my mother, Gülseren, my father, Dr. Burhan, and all my brothers for their tireless patience, continuous encouragement and great understanding during the whole of my graduate training and this thesis.

ABSTRACT

NUMERICAL MODELING OF NEARSHORE WAVE TRANSFORMATION USING THE MESHLESS MULTIQUADRIC METHOD

In the present study, nearshore wave transformation is numerically modeled using meshless multiquadric (MQ) method. The processes of water wave refraction, shoaling, breaking and re-forming; which are commonly observed in nature, are included in the model. Throughout the model development, plane bottom slope and periodic bottom topographies are handled separately. For all of the cases, an offshore boundary condition related to the wave angle is supplied to the model. Test results for the plane slope are verified using the analytical ones and yield highly favorable results. On the other hand, periodic bottom test results are compared with that of the REFDIF-1 outputs for the same case and the model results are proved to be satisfactory. Overall results demonstrate the meshless MQ method's ability to predict nearshore wave parameters with reasonable accuracy.

ÖZET

YAKIN KIYI DALGA TRANSFORMASYONUNUN AĞSIZ MQ YÖNTEMİ İLE SAYISAL MODELLENMESİ

Bu çalışmada yakın kıyı dalga transformasyonu ağsız MQ yöntemi ile sayısal olarak modellenmiştir. Doğada yaygın olarak görülen dalga sapması, sığlaşması, kırılması ve tekrar yapılanması süreçleri modele dâhil edilmiştir. Model boyunca düzgün taban eğimi ve periyodik taban topografyaları müstakil olarak ele alınmıştır. Her durumda, dalga açısı ile ilgili olmak üzere bir açık deniz sınır koşulu sağlanmıştır. Düzgün taban eğimine ait test sonuçları analitik sonuçlarla karşılaştırılmış ve çok başarılı sonuçlar elde edilmiştir. Diğer yandan, periyodik taban eğimi testinin sonuçları, aynı problem için çalıştırılmış REFDIF-1'in ürettiği çıktı ile kıyaslanmış ve model sonuçlarının tatmin edici olduğu görülmüştür. Bütün sonuçlar MQ yönteminin yakın kıyı dalga parametrelerini makul ölçüde tahmin edebildiğini göstermiştir.

TABLE OF CONTENTS

LIST OF FIGURES

LIST OF TABLES

LIST OF SYMBOLS

a	Amplitude of the periodic contour
B	Boundary condition operator
c	Radial basis function shape parameter
C	Wave phase velocity
C_0	Deep water wave speed
C_g	Group velocity
C_g^x	Derivative of the group velocity with respect to *x*
d	Water depth
d_b	Breaker water depth
d_i^x	Derivative of the water depth with respect to *x*, at node *i*
d_i^y	Derivative of the water depth with respect to *y*, at node *i*
E	Wave energy
f_{ij}	Entry of the multiquadric radial basis function matrix, at the *i*th row, *j*th column
f_{ij}^x	Entry at the *i*th row, *j*th column in the matrix for the derivative of the multiquadric with respect to *x*
f_{ij}^y	Entry at the *i*th row and *j*th column in the matrix for the derivative of the multiquadric with respect to *y*
f_{jk}^{-1}	Entry of the inverse of the multiquadric function matrix at *i*th row, *j*th column
g	Gravitational acceleration
H	Wave height
H_0	Deep water wave height
H_b	Breaker wave height
H^n	Wave height values at the *n*th iteration
k	Wave number

k_0	Deep water wave number
K	Decay coefficient
K_r	Refraction coefficient
K_s	Shoaling coefficient
L	Differential operator
L_0	Deep water wave length
m	Beach bottom slope
N	Number of collocation or data centers
N_b	Number of collocation centers on the offshore boundary
N_{bl}	Number of collocation centers on the breaker line
N_I	Number of internal collocation centers
p	Augmentation polynomial
$\boldsymbol{P_B}$	Matrix corresponding to the augmentation polynomials for the boundary equation
$\boldsymbol{P_L}$	Matrix corresponding to the augmentation polynomials for the field equation
q	Polynomial for the side conditions of the augmentation
r	Distance between two collocation centers
T	Wave period
u	Unknown function
u_a	Analytical solution of the unknown function
u_n	Numerical solution of the unknown function
u_{ϕ_i}	Approximate solution at the center i
x	Onshore direction
X_B	Indices for the collocation centers on the boundary
X_I	Indices for the interior collocation centers
y	Longshore direction
$\boldsymbol{\alpha}$	Vector of interpolation coefficients

α_j^{n+1}	Entry in the coefficient matrix of the *n+1*th iteration, at the *j*th row
α_s	Angle determining degree of skewness for the periodic bottom profile with skewed channel
Γ	Stable wave criterion coefficient
$\boldsymbol{\delta}$	Vector of coefficients of augmentation polynomials
δ	Energy dissipation rate
δ_b	Energy dissipation due to breaking
ζ	Anyone of the coordinate directions
θ	Wave angle
θ_0	Deep water wave angle
θ_b	Wave angle values along the offshore boundary
θ_i^x	Derivative of the wave angle with respect to *x,* at center *i*
θ_i^y	Derivative of the wave angle with respect to *y,* at center *i*
θ^n	Wave angle values at the *n*th iteration
κ	Spilling breaker constant
λ	Rip current spacing for the sinusoidal depth function
$\boldsymbol{\xi}$	Vector of boundary values
ξ	Right hand side of a boundary equation
ρ	Density of water
$\boldsymbol{\varphi}$	Vector of data values
φ	Right hand side of a field equation
Φ	Radial basis function
Φ_{ij}	Entry of the interpolation matrix at *i*th row, *j*th column
ω	Wave angular frequency
Ω	Problem domain
$\partial\Omega_b$	Offshore boundary
$\partial\Omega_{bl}$	Breaker line boundary

$\partial\Omega_l$	Left-side lateral boundary
$\partial\Omega_r$	Right-side lateral boundary
$\partial\Omega_s$	Shoreward boundary
$\partial\Omega$	Problem boundary

LIST OF ACRONYMS / ABBREVIATIONS

BC	Boundary condition
BEM	Boundary element method
BVP	Boundary value problem
deg	Degree
FDM	Finite difference method
FEM	Finite element method
GE	General equation
IC	Initial condition
MQ	Multiquadric
MQRBF	Multiquadric radial basis function
PDE	Partial differential equation
RBF	Radial basis function
RBFCM	Radial basis function collocation method

1. INTRODUCTION

1.1. Nearshore Wave Modeling in General

Numerous studies have been done with the aim of computing nearshore wave characteristics since it would serve as a basis during the planning of amphibious operations. These parameters include wave heights, wave propagation angles, longshore and cross-shore velocities, sand transport rates, beach profile changes, etc. Throughout the studies carried on during the past decades either analytical or numerical models are developed.

Earlier models like Collins (1970), Battjes (1972), Kuo and Kuo (1974) and Goda (1975) take into account only the local water depth during the shoaling process. However, latter models like the ones by Battjes and Janssen (1978), and Thornton and Guza (1983) are based on linear wave theory. These models and Svendsen (1984) were relatively simple models; require quick calculations and may be applied in a small amount of time. On the other hand, there are also more extensive models like SWAN and REFDIF. SWAN (Booij et al., 1999 and Ris et al., 1999) is a third generation wave model developed at Delft University of Technology. SWAN is a model that can be used to predict wave conditions varying slowly in space and time near coastal regions for environmental impact studies of sediment transport, shoreline transformation and marine disaster prevention (Wornom et al., 2001). It is a non-stationary spectral model which solves the spectral action balance equation representing the effects of spatial propagation; refraction; shoaling; generation; dissipation, for the evolution of wave growth. SWAN is presently integrated under the numerical Delft3D model. Unlike SWAN, REFDIF can also model diffraction. REFDIF-1 was originally developed by Kirby and Dalrymple (1983, 1985), as a monochromatic wave model. Subsequently a spectral version, REFDIF-S, is developed by Kirby and Tuba Ozkan (1994). In the past, ray-tracing techniques had been carried out to analyze refraction of water waves. These techniques have two main inadequacies: they supply data only on irregularly spaced rays and they can generate intersecting wave rays in shallow regions. Instead of using ray-tracing REFDIF develops a finite difference refraction model to provide wave heights and directions on a model grid. In 1992, Madsen and Sorensen

developed a Boussinesq model. It models the propagation of wind waves and swell from deep to shallow water over variable bathymetry counting on refraction, diffraction, shoaling, partial reflection and non- linear wave – wave interactions. However, it needs a great deal of data, can be applied to relatively small coastal regions and is limited to shallow depth ranges.

During the numerical computations included in the models, popularly used numerical techniques are the finite difference method (FDM), the finite element method (FEM) and the boundary element method (BEM). The FDM approximates differential operators by local algebraic ones valid at a series of usually uniformly spaced nodes within the solution domain. This aspect of the FDM makes it difficult to place nodes on the boundaries where boundary conditions are to be applied. The FEM assumes that the behavior of the system is duplicated on finite sized elements which when assembled approximate the solution domain. Both the FDM and FEM are thus domain discretization techniques. The BEM is an integral method based on integrating the governing equations over the solution domain. The result of such an operation involves only the values of the variables and their derivatives on the bounding curve or surface of the domain. Thus, the computer implementation of the BEM requires the boundaries of the system to be discretized into curve or surface elements. Above all meshing, especially of three-dimensional regions, is a time consuming, complicated task often requiring sophisticated software.

To avoid these drawbacks of the mesh-based methods a number of meshless methods have been developed during recent years. Among these, the radial basis function (RBF) collocation method (RBFCM), introduced by Kansa (1990a, 1990b), proved to be very efficient especially for solving partial differential equations (PDEs). The method is based upon the distances between collocation nodes, whose locations may be chosen randomly. The freedom in placing nodes makes the model highly flexible. Moreover, the RBFCM has been shown to be very accurate even for a small number of collocation points.

In the present study, the aim is to develop a numerical model based on RBF collocation to describe the transformation of waves entering shallow water. Refraction, shoaling, breaking and re-forming processes are included. As an ultimate target, nearshore wave height values are achieved.

The development of the model involved two phases. Initially, a beach of idealized shape is considered. Here a plane beach of constant slope is introduced. For the second phase, a longshore periodic bottom profile is implemented. Then, the model is tested wherever the analytical solutions are available. In addition, a comparison with the well-known wave model REFDIF-1 (detailed earlier in the first page), is done.

1.2. Transformation of Waves Entering Shallow Water

A number of changes occur as a train of waves propagates into shallow water. Among those, wave height variation is quite apparent. Waves near the breaker line are much higher than those farther offshore. Besides, wave direction undergoes change with shallower depths.

1.2.1. Refraction

Refraction is the change in direction of wave rays due to varying water depths. It is related to the difference in the velocities of wave crests. A wave crest in shallower water moves slower than that in deep water, enabling the deeper water wave crest to catch up. This makes wave crests become parallel to the shore as they propagate through the nearshore, tending to make the waves approach shore normally.

Consider a monochromatic linear wave propagating towards a shoreline as shown in Figure 1.1. The onshore direction is the x-direction, and the longshore direction is the y-direction. The angle θ is defined as the angle between the shore normal (x-coordinate) and the wave direction.

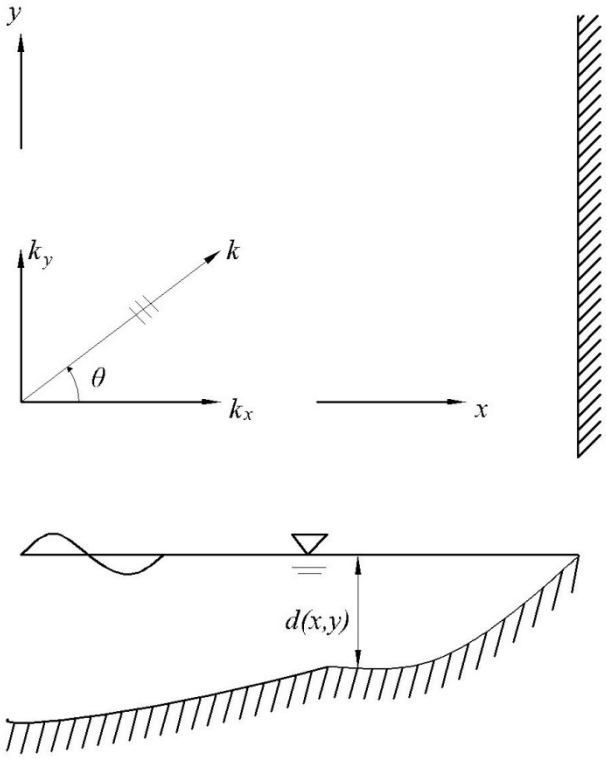

Figure 1.1. Definition sketch.

$\boldsymbol{k}$, shown in Figure 1.1, is described as the wave number vector which represents the wave number oriented in this direction. Referring to Dean and Dalrymple (1991), the irrotationality of the wave number vector requires that

$$\nabla \times \boldsymbol{k} = 0 \tag{1.1}$$

Substituting the *x* and *y* components of $\boldsymbol{k}$ yields

$$\frac{\partial}{\partial x}(ksin\theta) - \frac{\partial}{\partial y}(kcos\theta) = 0 \tag{1.2}$$

Expanding the derivatives gives

$$\left(\frac{\partial k}{\partial x}\sin\theta + k\cos\theta\frac{\partial \theta}{\partial x}\right) - \left(\frac{\partial k}{\partial y}cos\theta - k\sin\theta\frac{\partial \theta}{\partial y}\right) = 0 \tag{1.3}$$

This first-order nonlinear PDE should be solved to determine the wave angles for varying coordinates and water depths. Boundary conditions will be mentioned during the

problem definition. The wave number, *k*, and its derivatives, included in Equation 1.3, may be obtained by the use of wave dispersion equation, which is defined as

$$\omega^2 = gk \tanh kd \tag{1.4}$$

Here $\omega = 2\pi/T$ is the angular frequency, where *T* stands for wave period, and *d* is the local water depth. A two-dimensional schematic of wave characteristics is shown in Figure 1.2.

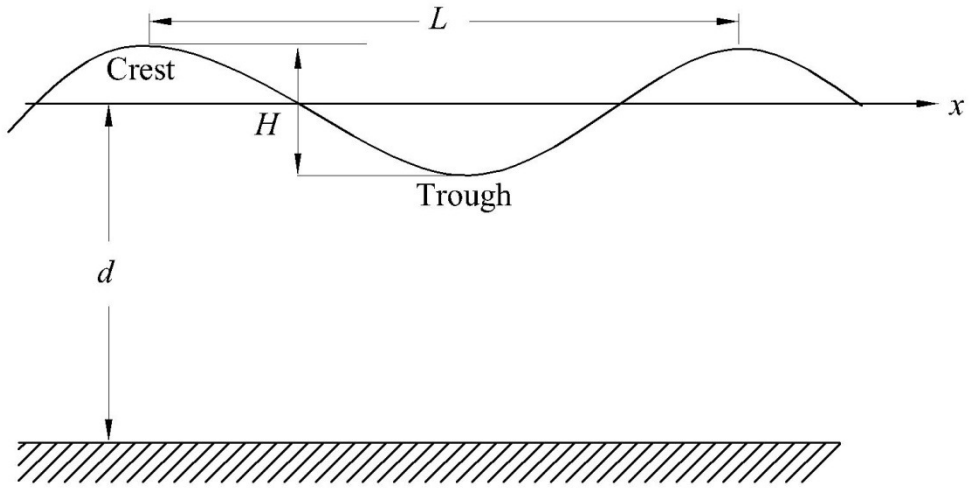

Figure 1.2. Wave Characteristics.

Equation 1.4 has one root, *k,* for given values of ω and *d*, which can be found by applying anyone of the root finding techniques like the one used in this study, the Newton - Raphson Method. To find the gradient of *k,* we rewrite the Equation 1.4 in the form of

$$\omega^2/g = k \tanh kd \tag{1.5}$$

Noting that the left hand side of the equation is a constant, since wave frequency is a constant, taking the gradient of both sides yields

$$\nabla(\omega^2/g) = (\tanh kd)\nabla k + (k \operatorname{sech}^2 kd)\nabla(kd) \tag{1.6}$$

or

$$0 = (\tanh kd)\nabla k + (k \operatorname{sech}^2 kd)(k\nabla d + d\nabla k) \tag{1.7}$$

There from we obtain gradients of k,

$$\nabla k = -\frac{k^2}{kd + \sinh kd \cosh kd} \nabla d \tag{1.8}$$

For the specific case where the bottom contours are straight and shore parallel, no longshore variation occurs, so the longshore gradients involved vanish. Then Equation 1.2 reduces to be

$$\frac{\partial (k \sin \theta)}{\partial x} = 0 \tag{1.9}$$

meaning that

$$k \sin \theta = \text{constant.} \tag{1.10}$$

The constant is evaluated in deep water, yielding Snell's Law:

$$k \sin \theta = k_0 \sin \theta_0 \tag{1.11}$$

where k_0 and θ_0 stands for the deep water wave parameters. Snell's Law enables us to analytically compute the local wave direction, θ, as the wave shoals, in the case of straight and shore parallel contours. Having knowledge of the analytical solution makes it possible to evaluate the numerical results and to compute errors.

1.2.2. Shoaling

Shoaling is defined as the process of wave height increase as the waves propagate towards shoreline over varying depths. This increase in wave height is related to increase in the energy per unit area of the wave. Considering wave heights at two points of interest, especially for the case of straight and parallel bottom contours as in Figure 1.3, the related equations can be developed. As there is no energy flux across the wave rays the energy flux across b_0 is the same as those across b_1 and b_2, shown in the Figure 1.3. Due to the convergence or divergence of the wave rays, resulting from either refraction or actual physical boundaries, and due to changes in depth, the energy per unit area changes between b_1 and b_2. Assuming no wave reflection, the conservation of energy requires,

$$(EnC)_1 b_1 = (EnC)_2 b_2 \tag{1.12}$$

Here *E* is the energy and *Cn* is the group velocity, the speed at which energy is transmitted. *ECn* is defined as the energy flux. Using the definition of energy,

$$E = \frac{1}{8}\rho g H^2 \tag{1.13}$$

we can solve for the wave height H_2:

$$H_2 = H_1 \sqrt{\frac{C_{g_1}}{C_{g_2}}} \sqrt{\frac{b_1}{b_2}} \tag{1.14}$$

where $C_g = Cn$ is the group velocity.

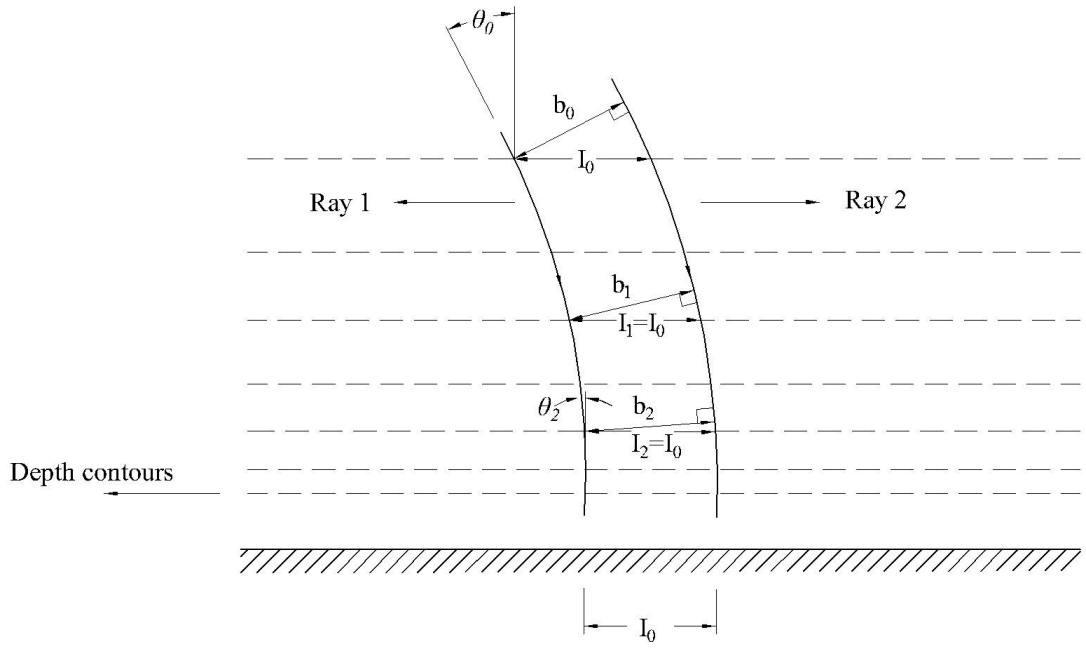

Figure 1.3. Characteristics of wave rays during refraction over idealized bathymetry.

Since the wave period is conserved, we have between deep and shallow water,

$$H_2 = H_0 \sqrt{\frac{C_0}{C_{g_2}}} \sqrt{\frac{b_0}{b_2}} \tag{1.15}$$

$$H = H_0 K_s K_r \tag{1.16}$$

where K_s is the shoaling coefficient and K_r is the refraction coefficient. From Figure 1.3 it can be seen that $b_0 = I_0 \cos\theta_0$ and $b_2 = I_0 \cos\theta_2$. Therefore the refraction coefficient, K_r, is

$$K_r = \left(\frac{b_0}{b_2}\right)^{1/2} = \left(\frac{\cos\theta_0}{\cos\theta_2}\right)^{1/2} \tag{1.17}$$

1.2.3. Breaking

At some depth, a wave of given characteristics will become unstable and break, dissipating energy in the form of turbulence and work against bottom friction, (Dean and Dalrymple,1991). The bottom slope and and the wave characteristics determine how the waves break. There are spilling, plunging and surging breakers. In this study, spilling breakers which occur typically on very mildly sloping beachs are used. For steeper beaches the waves are plunging breakers and if the slope is even more steeper, we have surging breakers.

The spilling breaker criterion, determined by McCowan (1894), gives that waves break when the ratio of the wave height to water the depth equals to 0.78. That is

$$H_b = \kappa d_b \tag{1.18}$$

where $\kappa = 0.78$, and H_b and d_b are the wave height and the water depth at the breaker line, respectively.

1.2.4. Waves after Breaking

There are a number of approaches to develop a rational model of wave height transformation across the surf zone. Mostly, the breaker height decay is based on the energy balance equation:

$$\frac{\partial(EC_g)}{\partial x} = -\delta(x) \tag{1.19}$$

in which δ is the energy dissipation rate per unit surface area due to boundary shear, and turbulence due to breaking. In this study, the only source of dissipation is taken to be that due to wave breaking. Referring to Kirby and Dalrymple (1986), who base their derivation on the detailed study of Dally et al. (1985), the expression for the dissipation term can be written as

$$\delta_b = \frac{KC_g}{d}\left(1 - \frac{\Gamma^2 d^2}{H^2}\right)E \tag{1.20}$$

where Γ and K are experimentally determined coefficients. Using Equation 1.13, for the definition of the wave energy E, Equation 1.19 may be rewritten as

$$\frac{\gamma}{8}\left(\boldsymbol{\nabla} H^2 \cdot \boldsymbol{C_g} + H^2 \boldsymbol{\nabla} \cdot \boldsymbol{C_g}\right) = -\delta_b \tag{1.21}$$

where $\gamma = \rho g$.

Separating the group velocity vector into its components, for a wave propagating at an angle θ to the onshore direction, gives

$$\boldsymbol{C_g} = \left(C_{g_x}, C_{g_y}\right) = \left(C_g \cos\theta\,, C_g \sin\theta\right) \tag{1.22}$$

Using the components of the group velocity in Equation 1.21 yields

$$-\delta_b \frac{8}{\gamma} = 2H\frac{\partial H}{\partial x} C_g \cos\theta + 2H\frac{\partial H}{\partial y} C_g \sin\theta + H^2\left[\frac{\partial}{\partial x}\left(C_g \cos\theta\right) + \frac{\partial}{\partial y}\left(C_g \sin\theta\right)\right] \tag{1.23}$$

or

$$\frac{\partial H}{\partial x} = -\frac{\partial H}{\partial y}\tan\theta - \frac{H}{2}\left[\frac{1}{C_g}\frac{\partial C_g}{\partial x} - \tan\theta\frac{\partial \theta}{\partial x}\right] - \frac{H}{2}\left[\frac{1}{C_g}\frac{\partial C_g}{\partial y}\tan\theta + \frac{\partial \theta}{\partial y}\right] - \frac{8}{\gamma}\delta_b \tag{1.24}$$

By using the definition of the group velocity vector, and taking the derivatives where necessary, the gradients of C_g can be determined to be

$$\begin{aligned}\frac{\partial C_g}{\partial x} &= C_0[\operatorname{sech}^2 kd](1 - kd\tanh kd)\frac{\partial (kd)}{\partial x}\\ \frac{\partial C_g}{\partial y} &= C_0[\operatorname{sech}^2 kd](1 - kd\tanh kd)\frac{\partial (kd)}{\partial y}\end{aligned} \tag{1.25}$$

Utilizing δ_b as given in Equation 1.20, Equation 1.24 becomes

$$\begin{aligned}\frac{\partial H}{\partial x} = &-\frac{\partial H}{\partial y}\tan\theta - \frac{H}{2}\left[\frac{1}{C_g}\frac{\partial C_g}{\partial x} - \tan\theta\frac{\partial \theta}{\partial x}\right] - \frac{H}{2}\left[\frac{1}{C_g}\frac{\partial C_g}{\partial y}\tan\theta + \frac{\partial \theta}{\partial y}\right]\\ &- \frac{K}{2\cos\theta}\left[\frac{H}{d} - \Gamma^2\frac{d}{H}\right]\end{aligned} \tag{1.26}$$

which is the general differential equation to be solved numerically to determine the wave decay across surf zone. There exist closed form solutions for cases of breaking on beaches of idealized bathymetry.

On a plane beach, where the water depth is changing linearly with distance *x*, given by

$$d(x) = d_b - mx \tag{1.27}$$

we have, (Dally et al., 1985),

$$\frac{H}{H_b} = \left[\left(\frac{d}{d_b}\right)^r (1+\alpha) - \alpha\left(\frac{d}{d_b}\right)^2\right]^{1/2} \tag{1.28}$$

where

$$\alpha = \frac{K\Gamma^2}{m\left(\frac{5}{2} - \frac{K}{m}\right)}\left(\frac{d}{H}\right)_b^2 \qquad r = \frac{K}{m} - \frac{1}{2} \tag{1.29}$$

The solution depends strongly on the values of K and Γ which are beach slope dependent. However, the single values $K = 0.15$ and $\Gamma = 0.40$ determined experimentally give satisfactory results for all beach slopes, (Dally et al., 1985).

1.3. Radial Basis Function Collocation Method

In recent decades, RBFs have been widely used for the solution of problems related to divergent scientific fields like computational mechanics, fluid dynamics, computer graphics and even economics. The main mathematical concepts, that are common among those fields, include recovery of functions from scattered data, meshless methods solving PDEs, ill posed and inverse problems, neural networks, and learning algorithms. All of these mentioned concepts can be handled easily and successfully by RBFs. For the theory of RBFs the reader is referred to the books of Buhmann (2003) and Wendland (2005). In addition, the book by Fasshauer (2007) covers the Matlab implementations of RBF based numerical methods.

The first attempt to use RBFs to solve PDEs is due to Kansa (1986), who makes use of Hardy's (1971) MQ interpolation. The studies of Kansa (1990a, 1990b) and Golberg and Chen (1996) demonstrate the effectiveness of the technique in solving PDEs. Hon et al. carried out extensive investigations to extend the applications to the numerical solutions of various ordinary and partial differential equations including general initial value problems (1997), the nonlinear Burger's equation (1998), the shallow water equation for tide and current simulation in domains with irregular boundaries (1993).

The RBFCM primarily focuses on construction of an unknown function from known data. This data includes the governing equations (GEs), boundary conditions (BCs) and initial conditions (ICs). Let $u(x, y, z)$ be an unknown function defined in the domain Ω and on the boundary $\partial\Omega$, and consider a boundary value problem (BVP) of the form

$$\begin{aligned} Lu &= \varphi \quad \text{in } \Omega \\ Bu &= \xi \quad \text{on } \partial\Omega \end{aligned} \tag{1.30}$$

where φ, ξ are known and, $\partial\Omega$ is the boundary of the region Ω. L is a differential operator and may be linear or non-linear, and B is a boundary condition operator. If L is non-linear a multilevel Newton iteration is required, and a linearized system is solved at each level.

The unknown solution, u, to PDE is approximated by a RBF, u_ϕ, of the form

$$u_{\phi_i} = \Phi_{ij}\alpha_j \qquad i,j = 1,\dots,N \tag{1.31}$$

for N number of nodes where u is to be approximated. Here, we let the collocation points (index i) be the same as the centers (index j) where the RBF's are located. α_j are the coefficients to be found, and $\Phi(r)$ is a radial basis function. r is the distance between two nodes given by

$$r = \sqrt{\left(x_i - x_j\right)^2 + \left(y_i - y_j\right)^2 + \left(z_i - z_j\right)^2} \tag{1.32}$$

The spatial derivatives of u can be obtained from Equation 1.31 as

$$\frac{\partial^n u_i}{\partial \zeta^n} = \frac{\partial^n \Phi_{\mathrm{ij}}}{\partial \zeta^n}\alpha_j \tag{1.33}$$

where ζ is any one of the coordinate directions x, y, or z, and at node i.

If L is time dependent then we let α be a function of time and solve for $\alpha(t)$ at discrete time steps. There are a number of RBFs, the most widely used ones are given in Table 1.1. Hardy (1968) demonstrated the success of the multiquadric RBF (MQRBF) in approximating randomly scattered data and it has been widely used for the solutions of PDEs. The continuous differentiability of the MQRBF makes it quite flexible, which allows the approximation of higher order derivatives. So, among the various RBFs it is reasonable to make use of MQ in this study too.

Table 1.1. Commonly used RBFs.

RBF	$\Phi(r)$
Multiquadrics (MQ)	$(r^2+c^2)^{\beta/2} \quad \beta>0, \beta \in 2N+1$
Inverse Multiquadric	$(r^2+c^2)^{-\beta/2} \quad \beta>0, \beta \in 2N+1$
Splines	$r^{\beta} \quad \beta>0, \beta \in 2N+1$
Thin Plate Splines (TPS)	$r^{\beta}\ln r \quad \beta>0, \beta \in 2N$
Gaussian	$\exp(-c^2r^2)$
*Wendland's compactly supported	$(1-r/R)_+^4(1+4r/R)$

*The subscript (+) means that the first term on the right hand side should be taken to be zero for $r > R$

Using Equation 1.31 and rewriting Equation 1.30 for N distinct points, then the collocation equations are

$$\begin{aligned}(L\Phi_{ij})\alpha_j &= \varphi_i \qquad i=1,\ldots,N_I, \quad j=1,\ldots,N \\ \left(B\Phi_{ij}\right)\alpha_j &= \xi_i \qquad i=1,\ldots,N-N_I, \quad j=1,\ldots,N\end{aligned} \tag{1.34}$$

where there are N_I internal nodes within the total of N nodes. This leads to the equivalent matrix equation

$$\begin{bmatrix}\boldsymbol{W_L}\\ \mathbf{W_B}\end{bmatrix}[\boldsymbol{\alpha}] = \begin{bmatrix}\boldsymbol{\varphi}\\ \boldsymbol{\xi}\end{bmatrix} \tag{1.35}$$

where

$$\begin{aligned}\boldsymbol{W_L} &= L\Phi_{\mathrm{ij}}\,, \quad i=1,\ldots,N_I, \quad j=1,\ldots,N \\ \boldsymbol{W_B} &= B\Phi_{\mathrm{ij}}\,, \quad i=1,\ldots,N-N_I, \quad j=1,\ldots,N\end{aligned} \tag{1.36}$$

The collocation matrix in Equation 1.35 has not been proven to be non-singular but it was shown by Schaback and Hon (2001) that finding a numerically singular matrix was very rare.

In fact, the form of the RBF approximation initially represented by Kansa (1990b) is

$$u_{\phi_i} = p_i + \Phi_{ij}\alpha_j \tag{1.37}$$

Here $p \in \mathbb{P}_k^d$ is a polynomial, augmented to the right-hand side of Equation 1.31. This is done with the aim of rendering the interpolation problem again uniquely solvable for the cases where the radial function Φ fails to be positive definite, (Buhmann, 2000). In this case, the collocation equations take the form of

$$\begin{aligned} Lp_i + (L\Phi_{ij})\alpha_j = \varphi_i \qquad & i = 1,\dots,N_I, \quad j = 1,\dots,N \\ Bp_i + (B\Phi)_{ij}\alpha_j = \xi_i \qquad & i = 1,\dots,N - N_I, \quad j = 1,\dots,N \end{aligned} \tag{1.38}$$

and the additional degrees of freedom are removed by the moment conditions

$$\alpha_j q_j = 0, \qquad \text{for all } q \in \mathbb{P}_k^d. \tag{1.39}$$

Then the collocation matrix comes to be

$$\begin{bmatrix} \boldsymbol{W_L} & \boldsymbol{P_L} \\ \boldsymbol{W_B} & \boldsymbol{P_B} \\ \boldsymbol{P^T} & \boldsymbol{0} \end{bmatrix} \begin{bmatrix} \boldsymbol{\alpha} \\ \boldsymbol{\delta} \end{bmatrix} = \begin{bmatrix} \boldsymbol{\varphi} \\ \boldsymbol{\xi} \\ \boldsymbol{0} \end{bmatrix} \tag{1.40}$$

where

$$\begin{aligned} \boldsymbol{P_L} &= Lp_i\,, \quad i = 1,\dots,N_I \\ \boldsymbol{P_B} &= Bp_i\,, \quad i = 1,\dots,N - N_I \end{aligned} \tag{1.41}$$

and $\left\{p_1, \dots, p_{\dim(\mathbb{P}_k^d)}\right\}$ forms a basis for $\mathbb{P}_k^d$. The vector $\boldsymbol{\delta}$ consists of coefficients with respect to this basis.

Although, this augmentation polynomial is included in the original definition of the RBF approximation, it is not included in this study (and in all applications done using a suitable RBF) since MQ is applicable without augmentation because of special properties of the function (Micchelli, 1986).

The form in Equation 1.31 is often called unsymmetric collocation (also referred to as Kansa's method) since the matrix in Equation 1.35 being unsymmetric. Therefore, there exists an alternative symmetric approach, which is in the form of

$$u_{\phi_i} = \sum_{j=1}^{N_I} (\hat{L}\Phi_{ij})\alpha_j + \sum_{j=N_I+1}^{N} (\hat{B}\Phi_{ij})\alpha_j \qquad i = 1, \dots, N \tag{1.42}$$

where $\hat{L}$ is the operator L, and $\hat{B}$ is the operator B now applied to the second argument (index j). Here the RBF is modified according to the locations of the collocation points (index j). Now the system matrix is

$$\begin{bmatrix} \boldsymbol{W_{L\hat{L}}} & \boldsymbol{W_{L\hat{B}}} \\ \boldsymbol{W_{\hat{L}B}^{T}} & \boldsymbol{W_{B\hat{B}}} \end{bmatrix} [\boldsymbol{\alpha}] = \begin{bmatrix} \boldsymbol{\varphi} \\ \boldsymbol{\xi} \end{bmatrix} \tag{1.43}$$

Here the inner matrices are

$$\begin{aligned} (W_{L\hat{L}})_{ij} &= L\hat{L}\Phi_{\mathrm{ij}}\,, & i,j \in X_I \\ (W_{L\hat{B}})_{i,j-N_I} &= L\hat{B}\Phi_{ij}\,, & i \in X_I \quad j \in X_B \\ (W_{\hat{L}B})_{i,j-N_I} &= \hat{L}B\Phi_{ij}, & i \in X_I \quad j \in X_B \\ (W_{B\hat{B}})_{i-N_I,j-N_I} &= B\hat{B}\Phi_{ij}\,, & i,j \in X_B \end{aligned} \tag{1.44}$$

where X_I and X_B represents the indices for the interior and boundary nodes, respectively. The main advantage of this formulation is that it is provably non-singular. However, symmetric RBF collocation is not as widely used as Kansa's unsymmetric method due to an extra application of L and B requiring RBF to be more differentiable. Also, it adds considerable complexity to the method.

2. NEARSHORE WAVE TRANSFORMATION PROBLEM

2.1. Objective and Scope

In this study, a numerical model using unsymmetric MQ method is developed to determine the nearshore wave characteristics: the local wave heights and the wave angles. The processes of refraction, shoaling, breaking and wave decay which lead to wave transformation are studied. The model includes two different phases related to different bottom profiles. For both of the models, Dirichlet boundary conditions are used offshore and the shape parameter, c, included in the MQ is taken to be a constant. In the first model, a plane bottom slope which has no longshore depth variation is used whereas in the latter one, a longshore periodic bottom profile is implemented. The calculation of wave parameters for both of the bottom profiles is handled in two stages. Firstly, refraction and shoaling processes are dealt with. Breaking is not considered at this first stage. At the offshore boundary deep water wave conditions are supplied to the model. Subsequent to the determination of the breaker line, the wave decay is modeled in the surf zone region, which extends from the breaker line to the dry beach. In this zone wave energy conservation is implemented as the GE and wave angles and wave heights at the breaker line are supplied as the BC. Both of the phases included are tested via comparison of the numerical results with the analytical ones, and the associated error values are inspected. A comparison with the widely used REFDIF-1, combined refraction diffraction model is also performed. Ultimately, it is shown that the MQ method provides a good alternative way of modeling nearshore wave transformation phenomena.

2.2. Assumptions

The following general assumptions are imposed in the models.

- The fluid is homogeneous, inviscid and incompressible.
- The flow is irrotational.
- There is no generation or dissipation of wave energy, outside of the surf zone. The only energy dissipation within the surf zone is due to wave breaking.

- Bottom friction is neglected.
- Wave – current interaction is neglected.
- Wave induced set-up and set-down are not included.

2.3. Problem Definition

Problem definitions for straight and shore parallel contour, and for longshore periodic bottom profile cases are interpreted separately as changes occur in the GEs. Firstly, refraction problem which is modeled to determine the local wave angles, is defined. Then, local wave heights are computed using these angles in the expression resulting from the wave energy conservation. Wave height computation differs for the surf zone region since energy dissipation due to breaking occurs here. Problem definition for the surf zone region is given after the refraction problem.

2.3.1. Straight and Shore Parallel Contours

To compute the refraction of waves, problem can be defined in a domain Ω and an offshore boundary of $\partial\Omega_b$. For all the other three boundaries, $\partial\Omega_s, \partial\Omega_r, \partial\Omega_l$, of the region, GE is applied. A visual representation of the problem is included in Figure 2.1. Using Equation 1.3, the expansion for $\nabla \times k = 0$, and remembering that longshore gradients of the variables vanish in the absence of longshore variation, the problem can be defined as

$$\begin{aligned} \frac{\partial k}{\partial x}\sin\theta + k\cos\theta\frac{\partial \theta}{\partial x} = 0 \qquad & \text{in } \Omega, \text{ and on } \partial\Omega_s, \partial\Omega_r, \partial\Omega_l \\ \theta = \theta_b \qquad & \text{on } \partial\Omega_b \end{aligned} \tag{2.1}$$

where k is the wave number vector, θ is the wave angle, and θ_b are the wave angles along the offshore boundary. These wave angles are supplied by the use of Snell's law, Equation 1.11, which takes deep water parameters as input, and outputs the local wave angles.

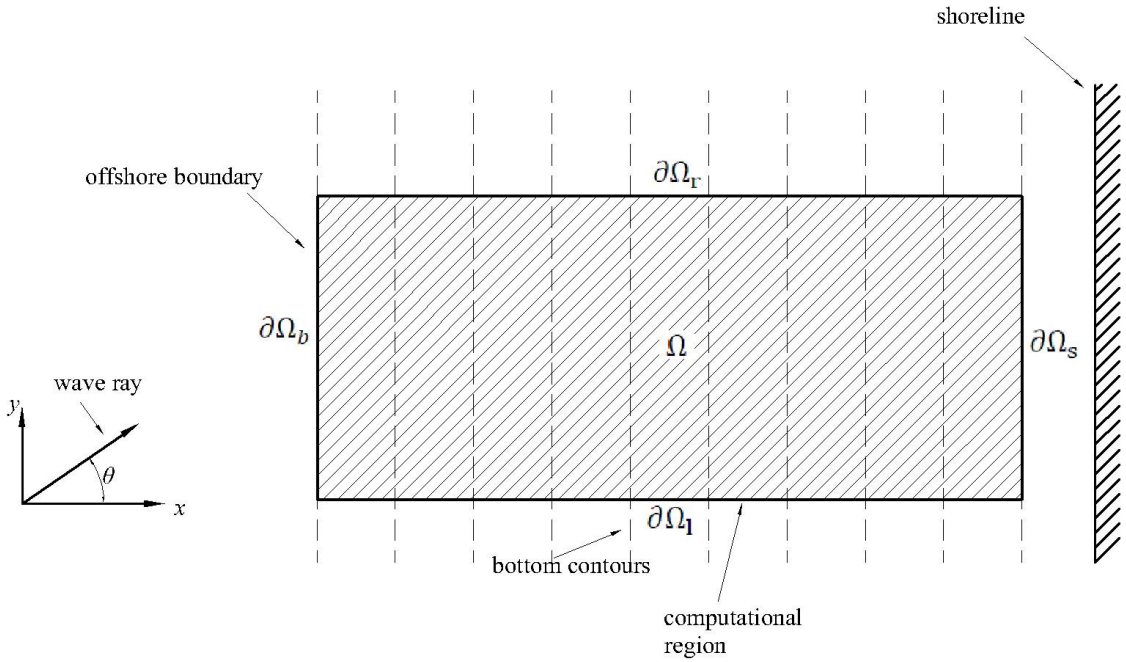

Figure 2.1. Schematic illustration of beach terminology and computational region.

Wave heights are computed by the use of Equation 1.16. Thereafter, spilling breaker criterion, Equation 1.18, is used to determine the breaking wave height.

The surf zone wave decay problem is defined using Equation 1.26 and excluding longshore gradients, as

$$\frac{\partial H}{\partial x} = -\frac{H}{2}\left[\frac{1}{C_g}\frac{\partial C_g}{\partial x} - \tan\theta\frac{\partial \theta}{\partial x}\right] - \frac{K}{2\cos\theta}\left[\frac{H}{d} - \Gamma^2\frac{d}{H}\right] \quad \text{in } \Omega, \text{ and on } \partial\Omega_s, \partial\Omega_r, \partial\Omega_l$$
$$H = H_b \quad \text{on } \partial\Omega_{bl} \tag{2.2}$$

where H is the local wave height, C_g is the group velocity, d is the local water depth, and K and Γ are constants. Here, $\partial\Omega_{bl}$ is the breaker line as the boundary, Ω is the interior region and all the remaining three boundaries are $\partial\Omega_s, \partial\Omega_r, \partial\Omega_l$, as illustrated in Figure 2.2. Lastly, H_b is the breaking wave height, which is the same along the breaker line.

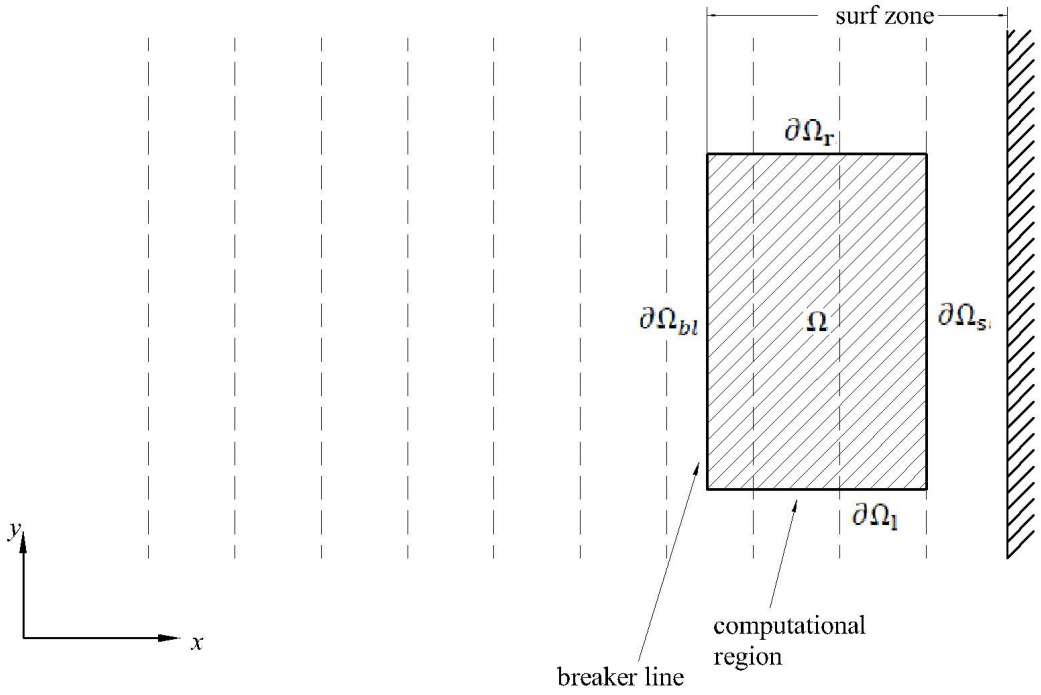

Figure 2.2. Schematic illustration of the surf zone and computational area.

2.3.2. Variable Bottom Topography

The same procedure is applied to define the problem for the longshore periodic bottom profile. For the functions Noda (1974) is referred to, who introduced three different longshore periodic depth functions. The first is a sinusoidal function, defined as

$$d(x,y) = m[x - a\sin(2\pi y/\lambda)] \tag{2.3}$$

where a is the amplitude of the periodic contour and λ is the wavelength physically associated with rip current spacing. A second depth function for a periodic beach is given by

$$d(x,y) = mx\left[1 + a\exp\left(-x^{1/3}/b\right)\cdot\sin^{10}(\pi y/\lambda)\right] \tag{2.4}$$

Lastly, a periodic beach topography with skewed channels is described by

$$d(x,y) = mx\left[1 + a\exp\left(-x^{1/3}/b\right)\cdot\sin^{10}\left(\frac{\pi}{\lambda}(y - x\tan\alpha_s)\right)\right] \tag{2.5}$$

The bottom profiles for the three cases; sinusoidal, periodic, and periodic with skewed channel, are illustrated in Figure 2.3.

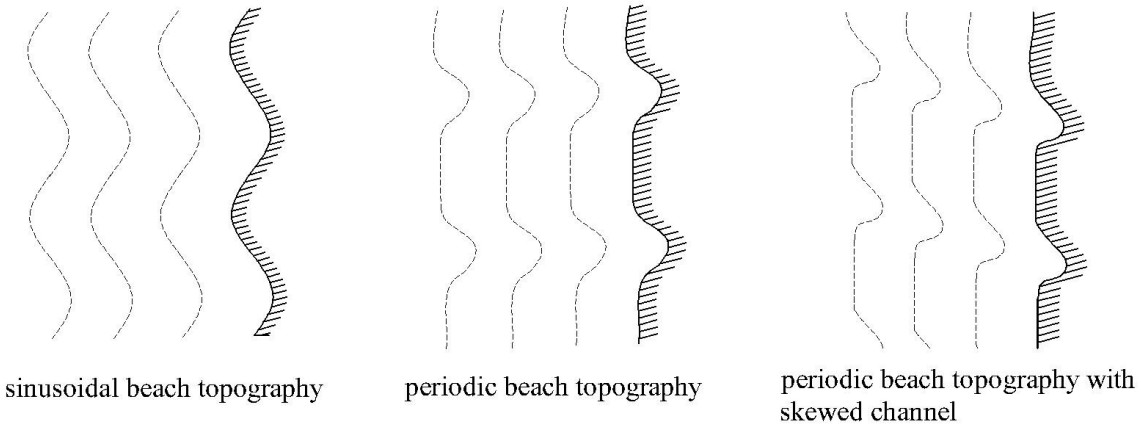

Figure 2.3. Beach topographies used in the model.

The GEs for refraction and the surf zone are similar to those of the plane beach problem. Now, the depth contours are not straight, which requires longshore gradients also to be involved in the equations. Computational regions are the same as before (Figures 2.1 and 2.2). To determine the wave angles, the BVP may be given as

$$\left(\frac{\partial k}{\partial x}\sin\theta + k\cos\theta\frac{\partial \theta}{\partial x}\right) - \left(\frac{\partial k}{\partial y}cos\theta - k\sin\theta\frac{\partial \theta}{\partial y}\right) = 0 \quad \text{in} \quad \Omega,\ \partial\Omega_{\mathrm{s}}, \partial\Omega_{\mathrm{r}}, \partial\Omega_{\mathrm{l}}$$
$$\theta = \theta_{\mathrm{b}} \quad \text{on} \quad \partial\Omega_{\mathrm{b}} \tag{2.6}$$

The notation, for the boundaries and the interior region, is same as before. Wave angles for the offshore boundary are supplied using Snell's Law. Although a longshore variation exists here, Snell's Law still can provide reasonable boundary wave angle values, since it behaves pointwise and since the model would start in intermediate water where the bottom does not have a significant effect on the wave parameters.

Once again the wave heights are determined using Equation 1.16, and the breaker line is determined using spilling breakers criterion.

The problem for the surf zone is defined using the full form of Equation 1.26; the equation resulting from the expansion for the wave energy flux conservation equation. It is rewritten as the GE

$$\begin{aligned} &\text{Equation 1.26} && \text{in } \Omega,\ \partial\Omega_{\mathrm{s}}, \partial\Omega_{\mathrm{r}}, \partial\Omega_{\mathrm{l}} \\ &H = H_b && \text{on } \partial\Omega_{bl} \end{aligned} \tag{2.7}$$

The notation, for the interior region and the boundaries, is same as for the straight and shore parallel case. But, now breaker wave height values wouldn't be the same along the breaker line since we have a variable bottom topography instead of a straight and parallel one.

3. NUMERICAL FORMULATION

A numerical model using the RBFCM is developed which is capable of describing the two-dimesional problem related to wave refraction and transformation of wave height due to shoaling, breaking and re-forming processes. The two cases of straight-parallel contours and periodic bottom profiles are examined separately. It should be remembered that the onshore direction is the *x*-direction and while the longshore one is the *y*-direction. MQ is used as the radial basis function throughout the model.

3.1. Straight and Shore Parallel Contours

In order to model refraction, which gives the local wave directions, the angle between the wave ray and the *x*-direction, θ, is approximated as

$$\theta_i = f_{ij}\alpha_j\,, \qquad i,j = 1,\dots,N \tag{3.1}$$

where α's are the constants, and N represents the total number of nodes included in the model. θ_i is the wave angle for the ith center located at (x_i, y_i). f_{ij} is the RBF matrix with elements of MQs defined as

$$f_{ij} = \sqrt{\left(x_i - x_j\right)^2 + \left(y_i - y_j\right)^2 + c^2} \tag{3.2}$$

where c is the shape parameter.

Subsequent to determination of the coefficients for each point, the gradients for the wave angle can be simply denoted as

$$\theta_i^x = f_{ij}^x \alpha_j \tag{3.3}$$

$$\theta_i^y = f_{ij}^y \alpha_j \tag{3.4}$$

Clearly, θ_i^x and θ_i^y are the *x* and *y* derivatives of the local wave angle, respectively. Same notation is used for the RBF derivatives too. Though illustrated, y- derivatives are not used for this plane bottom case.

In order to model refraction the GE included in Equation 2.1 is rewritten as

$$\frac{\partial \theta}{\partial x} = -\frac{1}{k}\frac{\partial k}{\partial x}\tan\theta \tag{3.5}$$

An iterative solution of the form,

$$\frac{\partial \theta^{n+1}}{\partial x} = -\frac{1}{k}\frac{\partial k}{\partial x}\tan\theta^{n} \tag{3.6}$$

is considered, where *n* stands for the iteration number. Equation 1.5 and 1.8 are used to supply wave number and its gradient at each point of the computational region. Lastly, the model for refraction comes to be in the form of

$$\begin{aligned} f_{ij}\alpha_j &= \theta_b\,; && i = 1,\dots,N_b \quad j = 1,\dots,N \\ f_{ij}^x\alpha_j^{n+1} &= \left(-\frac{1}{k}\frac{\partial k}{\partial x}\right)_i \tan\theta_i^n\ ; && i = 1,\dots,N-N_b \quad j = 1,\dots,N \end{aligned} \tag{3.7}$$

where θ_b, is the wave angles on the offshore boundary and N_b is the number of offshore boundary nodes included.

The next region of the numerical model is the surf zone region, in which the GE and the BC differs from that of the refraction model. Now, the wave heights are to be determined. Therefore, the wave height, *H*, is approximated as

$$H_i = f_{ij}\alpha_j\,, \qquad i,j = 1,\dots,N \tag{3.8}$$

For numerical modeling of surf zone wave height decay, again an iterative solution is considered;

$$\frac{\partial H^{n+1}}{\partial x} = -\frac{H^n}{2}\left[\frac{1}{C_g}\frac{\partial C_g}{\partial x} - \tan\theta\frac{\partial \theta}{\partial x}\right] - \frac{K}{2\cos\theta}\left[\frac{H^n}{d} - \Gamma^2\frac{d}{H^n}\right] \tag{3.9}$$

Therefore, the numerical model of the problem defined in Equation 2.2 takes the form

$$\begin{aligned} & f_{ij}\alpha_j = H_b\ ; && i = 1,\ldots,N_{bl} \quad j = 1,\ldots,N \\ & f_{ij}^x\alpha_j^{n+1} = -\frac{H_i^n}{2}\left[\left(\frac{1}{C_g}C_g^x\right)_i - \tan\theta_i\,\theta_i^x\right] && \\ & \quad -\frac{K}{2\cos\theta_i}\left[\frac{H_i^n}{d_i} - \Gamma^2\frac{d_i}{H_i^n}\right]; && \begin{matrix} i = 1,\ldots,N - N_{bl} \\ j = 1,\ldots,N \end{matrix} \end{aligned} \tag{3.10}$$

where N_{bl} is the number of nodes on the breaker line, which is now the seaward boundary of the surf zone region, and H_b are the wave heights on this boundary, predetermined by the spilling breaker criterion. It should be noted that the wave angles, included in Equation 3.10, are determined previously from the solution of the refraction model. Additionally, gradients of θ may be determined by the use of Equations 3.1 and 3.3, so that

$$\vec{\nabla}\theta_i = \vec{\nabla}f_{ij}\alpha_j = \vec{\nabla}f_{ij}f_{jk}^{-1}\theta_k \tag{3.11}$$

Moreover, gradients of d, included in the computation of the gradients of $C_g$are also obtained in the same manner as above. That is, assuming that $d_i = f_{ij}\alpha_j$, and recalling Equations 3.3 and 3.4, the gradients of depth can be achieved as

$$d_i^x = f_{ij}^x f_{jk}^{-1} d_k \tag{3.12}$$

$$d_i^y = f_{ij}^y f_{jk}^{-1} d_k \tag{3.13}$$

3.2. Variable Bottom Topography

The numerical model of the periodic bottom topography is broadly similar to that of the previous case, except for the longshore gradients involved in the associated equations. The GE included in Equation 2.6, which is to be solved iteratively, may be written in the alternative form of

$$\frac{\partial \theta^{n+1}}{\partial x} = \frac{1}{k}\frac{\partial k}{\partial y} - \tan\theta^n \frac{\partial \theta^n}{\partial y} - \tan\theta^n \frac{1}{k}\frac{\partial k}{\partial x} \tag{3.14}$$

in which all terms other than the *x*-derivative of the wave angle are grouped in the right-hand side of the equation. The wave angle is again approximated as given in Equation 3.1. Therefore, the refraction model for the periodic bottom case comes to be

$$\begin{aligned} & f_{ij}\alpha_j = \theta_b\ ; && \begin{matrix} i = 1,\ldots,N_b \\ j = 1,\ldots,N \end{matrix} \\ & f_{ij}^x \alpha_j^{n+1} = \left(\frac{1}{k}\frac{\partial k}{\partial y}\right)_i - \left(\frac{1}{k}\frac{\partial k}{\partial x}\right)_i \tan\theta_i^n - \tan\theta_i^n\, f_{ij}^y \alpha_j^n\ ; && \begin{matrix} i = 1,\ldots,N-N_b \\ j = 1,\ldots,N \end{matrix} \end{aligned} \tag{3.15}$$

where the longshore gradient of the wave angle is approximated using Equation 3.4.

Wave heights for the surf zone are approximated as indicated in Equation 3.8. Wave decay is handled by updating the model included in Equation 3.10 to adapt Equation 2.7. Thereafter, RBFCM model for the wave heights takes the form of

$$\begin{aligned} & f_{ij}\alpha_j = H_b\ ; && \begin{matrix} i = 1,\ldots,N_{bl} \\ j = 1,\ldots,N \end{matrix} \\ & f_{ij}^x \alpha_j^{n+1} = -f_{ij}^y \alpha_j^n \tan\theta_i - \frac{H_i^n}{2}\left[\left(\frac{1}{C_g}C_g^x\right)_i - \tan\theta_i\,\theta_i^x\right] \\ & \qquad - \frac{H_i^n}{2}\left[\left(\frac{1}{C_g}C_g^y\right)_i \tan\theta_i + \theta_i^y\right] && i = 1,\ldots,N-N_{bl} \\ & \qquad - \frac{K}{2\cos\theta_i}\left[\frac{H_i^n}{d_i} - \Gamma^2\frac{d_i}{H_i^n}\right]; && j = 1,\ldots,N \end{aligned} \tag{3.16}$$

Again gradients of θ are determined utilizing the approach outlined in Equation 3.11.

4. NUMERICAL TESTS AND RESULTS

In order to examine the efficiency of the model developed some numerical tests are conducted. For both of the bottom profiles, plane and periodic profiles, included in the model, a monochromatic wave with 10s period is propagated. It should be remembered that the *x*-direction was taken to be the onshore direction while the *y*-direction to be the longshore one. It also should be noted that shape of the shoreline is exactly the same as the associated bottom profile. Node numbering is made such that the offshore contour is the first contour and includes the first ten nodes, and the shoreward contour is the last contour, including the last ten nodes. The Newton – Raphson method is used to solve the wave dispersion equation (Equation 1.4) to determine the local wave numbers, *k*. Deep water wave parameters of $\theta_0 = 60^{\circ}$ and $H_0 = 3\text{m}$ are also supplied to the model. The shape parameter, appearing in MQs, is taken to be a constant, $c = 90$, through nearly all the phases of the model. This value was determined to be the best fit after several trials. c value should be chosen in accordance with the distribution of the centers, that is to say; for the cases where the inter-nodal distance is relatively small, less than 10m for instance, then a small value of *c*, such as 9, would be a good choice; whereas for distances that are greater than that then a larger value for *c*, such as 90, would work. During the trials using various shape parameters the known fact is achieved, which says that higher values of *c* would improve the results within the same contour, and on the other hand, lower values of *c* value would eliminate the singularity, if exists, of the system matrix included in RBF model. However, once the model works with reasonable accuracy, say with an error less than 1%, then no further significant reduction in error values can be achieved using different *c* values. Among the various tests only for the mesh-free test case, a different c value is used. A value of 1000 is employed here. This increment in the shape parameter comes to be essential when the node distribution is free of any meshes. Lastly, for the constants K and Γ included in the modeling of surf zone area, the values of 0.15 and 0.40 – with an ∓ 0.02 change – are used, respectively. Numerical results are compared with that of the analytical ones, wherever possible. In addition, same problem is solved and associated wave parameters are obtained by the use of widespread wave model REFDIF. Thereby, a comparison between the model developed in this study and the model of REFDIF is made.

All the numerical calculations are performed using Matlab 7.1 on a laptop computer with a Dual-Core Processor.

4.1. Straight and Shore Parallel Contours

During the first phase of the study, a linear bathymetry is used where depth values change linearly from 10m for the seaward contour to 1m for the shoreward contour, over a 0.1 beach slope. A total of 100 uniformly placed nodes are used within a square computational region, meaning that *x* and *y* directions include equal number of nodes. This node placement is used for all tests except when the model is tested using a random node distribution. The details related to this test will be given later. A zone extending 100m in the onshore – offshore direction is examined. A two dimensional model is important to see the changes in wave parameters within the same contour, where actually no change should occur since depth values are the same for the same contour. Firstly, the model for the wave refraction is tested. The wave angle variation within the contours is sought since the model should find very close angle values for the same contour. Figure 4.1 shows the longshore variation of wave angles for different depth contours. The model does a better job of approximating wave angles in the interior of the domain than in regions close to the boundaries. Nevertheless, it is achieved that the variation in any contour does not exceed 0.02 % ; so little that the variation lines are almost horizontal.

In the analysis of the model results, RMSE values are calculated where necessary in order to obtain an overall indicator of the error. The RMSE is defined as

$$RMSE = \sqrt{\frac{\sum_{i=1}^{N}(u_a - u_n)_i^2}{N}} \tag{4.1}$$

where u_a is the exact solution and u_n is the numerical one. N stands for the number of total nodes used.

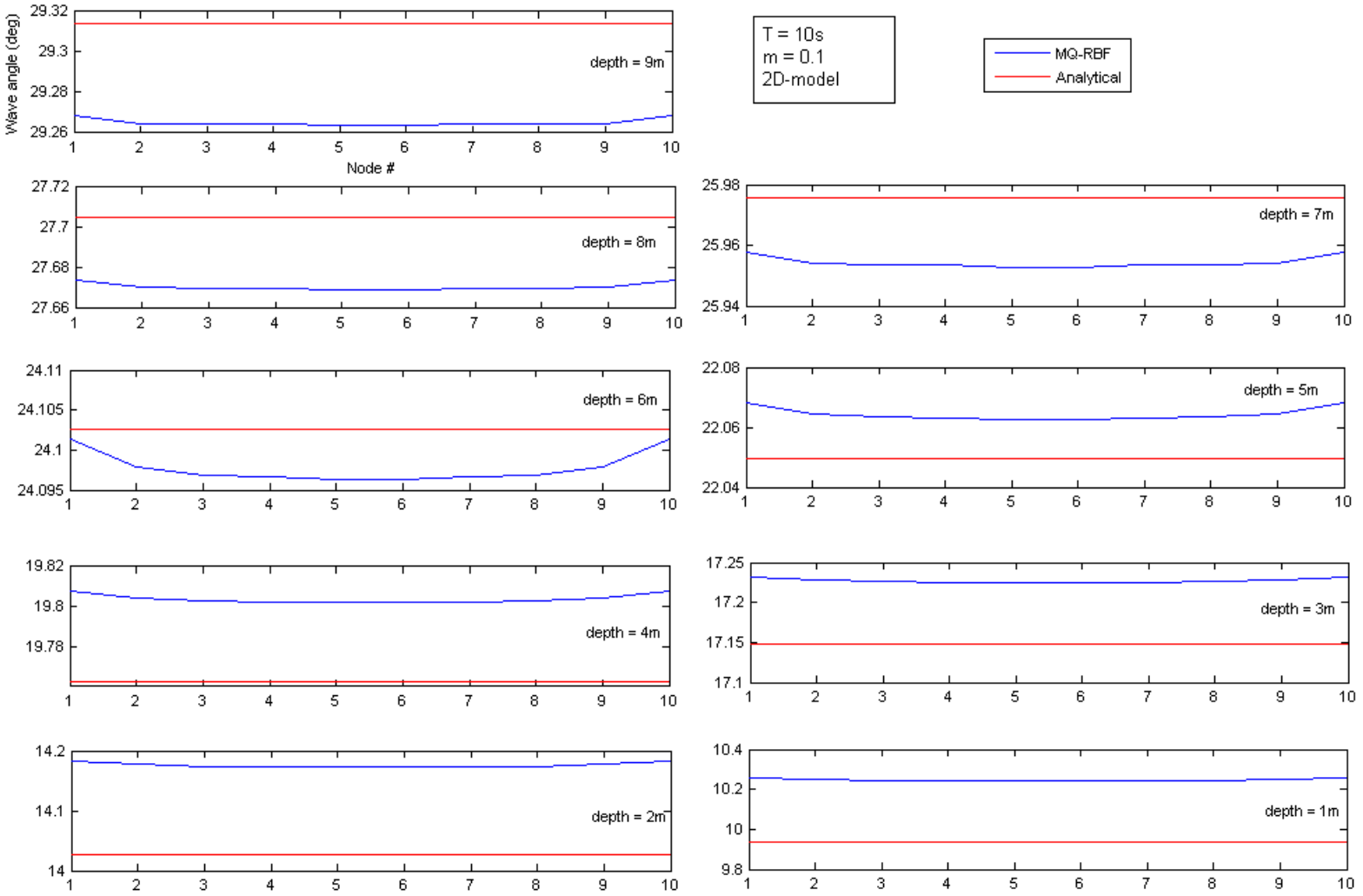

Figure 4.1 Longshore variation in wave angle values, for different depth contours.

Figure 4.2 shows the distribution of the error values in the computational region. It shows that the model more successfully predicts the wave angles for the interior nodes than for the lateral boundary nodes. Again, although an error increase exists in the regions adjacent to the lateral boundaries, the model still makes a highly reasonable estimate, namely an average relative error of 0.6 %, for these regions too.

Table 4.1 shows the error results of the refraction model for $y = 0$ - onshore transect. Since the longshore behavior of the model is analyzed previously, it would be sufficient to use one-dimensional onshore-results for the refraction process. Wave angles are in degrees. *Abs-err* and *% err* stand for absolute error and relative error, respectively. It can be observed that the process is accurately modeled and that it gives the expected wave angle decrease towards shore. Again, error values become higher approaching seaward and shoreward boundaries. Even within these regions, the model is able to reliably predict the parameter with a maximum relative error of 3 %. Figure 4.3 is a graphical representation of numerical vs. analytical wave angle values. Figure 4.4 is a vector plot of the wave refraction process.

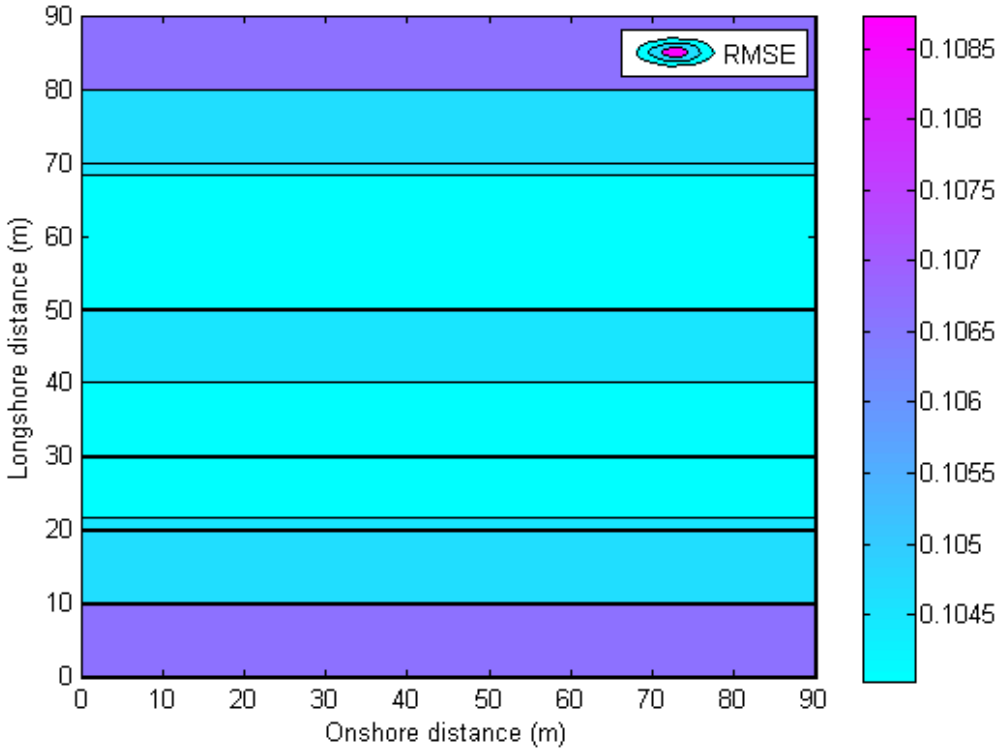

Figure 4.2. Wave angle RMSE (deg) for different onshore rows.

Table 4.1. Numerical and analytical wave angles, and associated error values.

Depth (m)	θ- analytical (deg.)	θ- numerical (deg.)	abs-err	% err
10	30.0009	30.0009	0.0000	-0.0001
9	28.5409	28.4939	0.0469	0.1644
8	26.9811	26.9487	0.0324	0.1199
7	25.3040	25.2835	0.0204	0.0807
6	23.4854	23.4809	0.0045	0.0190
5	21.4906	21.5048	0.0142	-0.0659
4	19.2662	19.3062	0.0400	-0.2075
3	16.7220	16.7980	0.0760	-0.4543
2	13.6826	13.8245	0.1420	-1.0375
1	9.6948	9.9895	0.2947	-3.0394

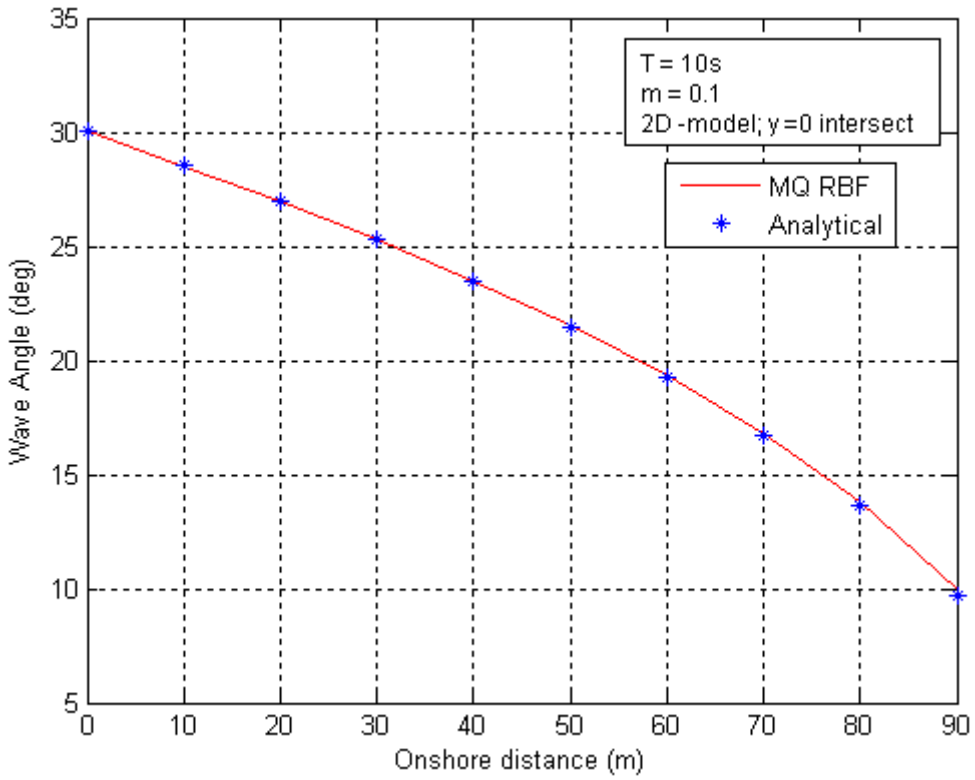

Figure 4.3. Analytical vs. numerical wave angle values.

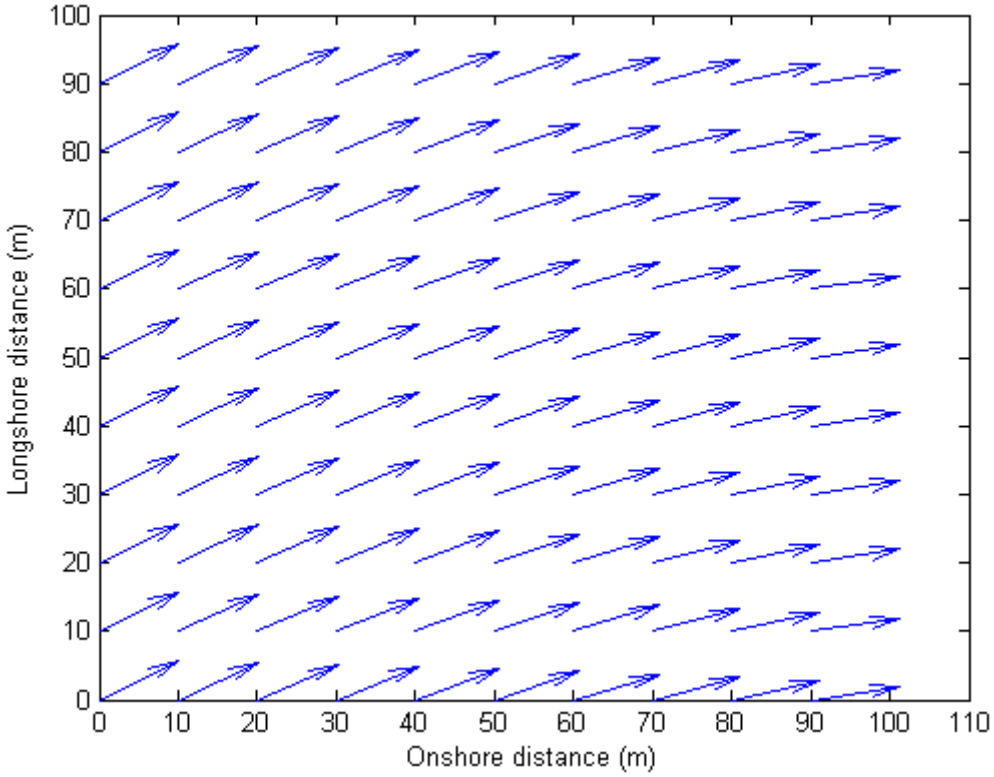

Figure 4.4. Wave refraction.

A sensitivity analysis is also conducted to investigate the behavior of the model. There are three distinct variables that are supplied to the model as an input. These are the wave period, T; the wave steepness, H_0/L_0; and the deep water wave angle, θ_0. To examine how well the model works for different values of these variables, three separate tests are performed. During all the tests a bottom slope of 0.1 is used. Throughout the sensitivity analysis process, the outer model which approximates the wave angle values due to refraction, and the inner model which predicts the surf zone wave height values are dealt with separately. For the first case, the wave period and the wave steepness are taken to be constants and deep water wave angle values of 0° to 89°, with a 10° increment between successive angles, are tried out. Offshore boundary wave angles range from 0° to 56.6122° for 2s wave period and from 0° to 30.2556° for 12s wave period, for successive trials, respectively. Although a 89° deep water wave angle is unrealistically high, it is used to show that the model works even for such a high value, which implies that the model will already work for lower deep water wave angle values. For each case, the associated RMSE values are computed. The same process is repeated for two different wave period and wave steepness values: $T = 2\text{s}$ and 12s; and $H_0/L_0 = 0.01$ and 0.142. For the first test, the sensitivity of the results to wave angle is examined. Different domains are used for the two

wave periods to be able to include the shallow water region. Table 4.2 shows the change in the RMSE values of the wave angle due to a change in θ_0. For all of the four cases an increasing trend in error values can be observed. So, the model works better at low values of $\theta_0$for both of the wave periods. But, in the higher wave period, a more rapid increase can be seen. However, it can be inferred that the model still makes a highly reasonable estimate of the parameter in each case. Another outcome of this test is that the wave refraction error values are insensitive to the wave steepness. Table 4.3 shows the change in the RMSE of the inner model due to a change in θ_0. As mentioned, the inner model approximates the wave height values in the surf zone. For the first plot in Table 4.3, where $T = 2$ and $H_0/L_0 = 0.142$, breaking occurs when θ_0 values are larger than $40°$. So, for all the plots in this table the error change can be plotted only for cases where a surf zone exists. From the four graphs in Table 4.3 it can be concluded that the model predicts the surf zone wave heights generally with a higher accuracy for larger values of θ_0.

Table 4.2. Wave angle RMSE change due to change in deep water wave angle.

H0/L0	
0.142	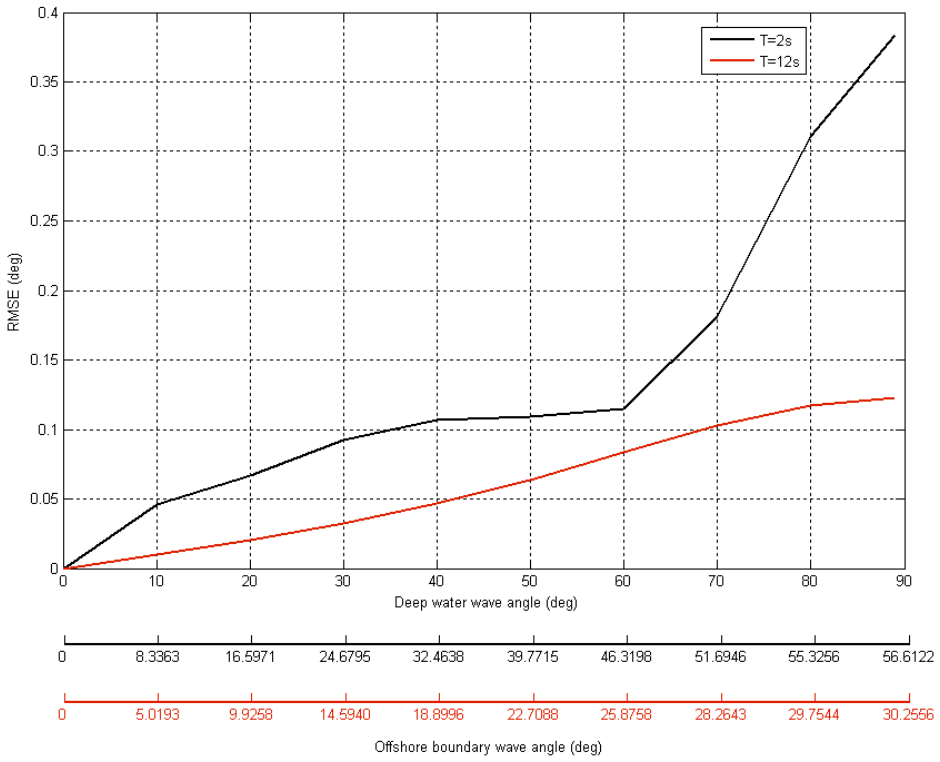
0.01	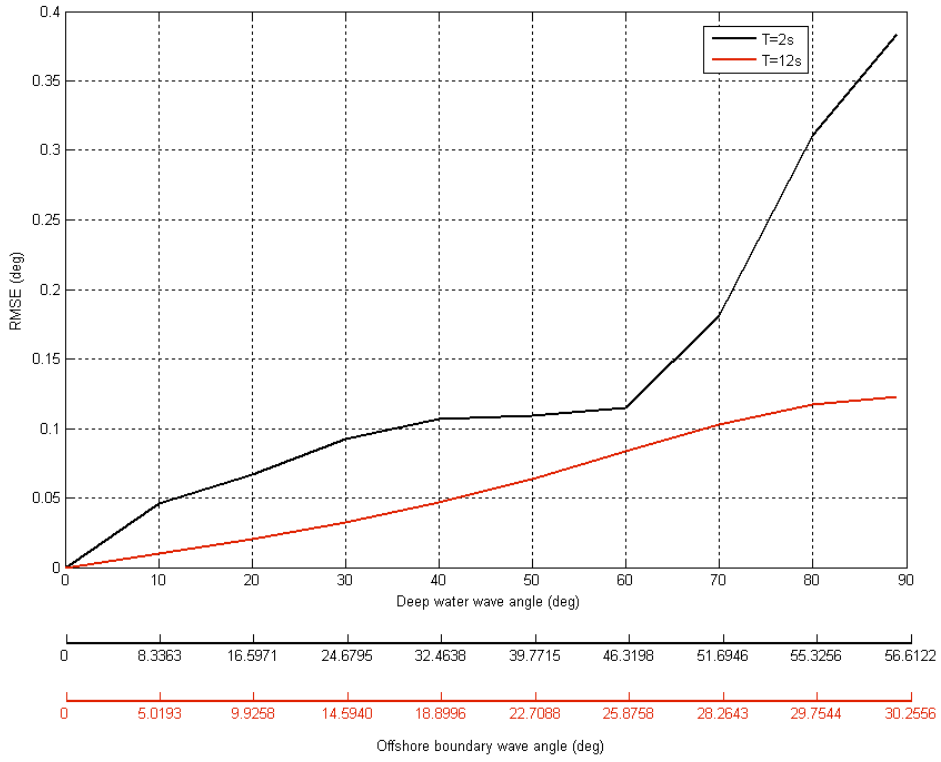

Table 4.3. Surf zone wave height RMSE change due to change in deep water wave angle.

T	2	12	H0/L0
	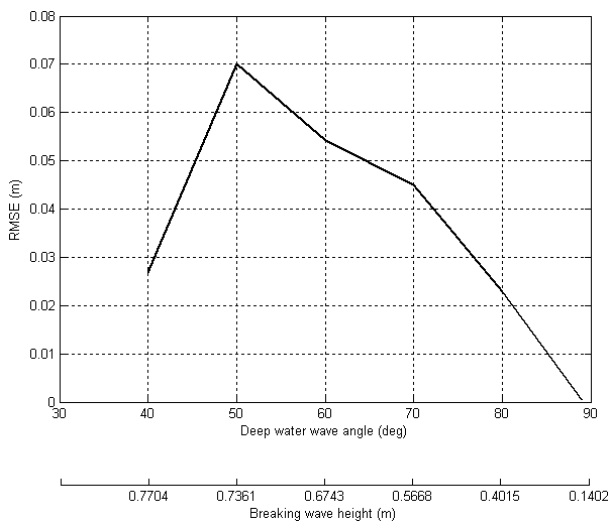		**0.142**
	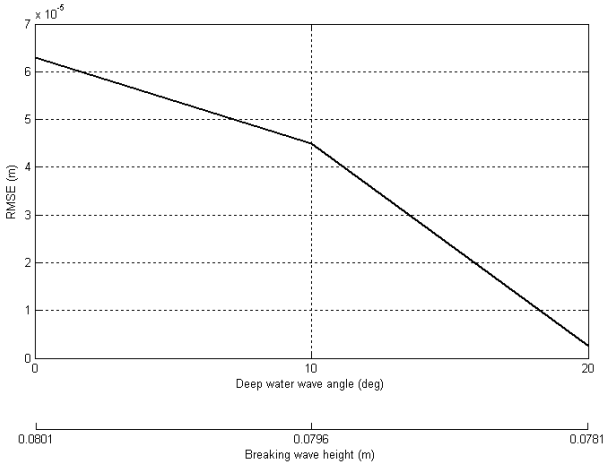	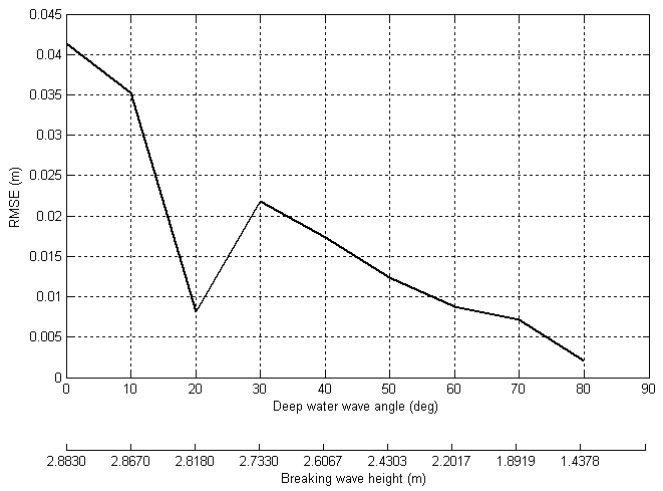	**0.01**

For the next test, the wave steepness and the deep water wave angle are taken as constants while wave period values are changed from $T = 2$ to 12 seconds with an increment of 2 seconds. Again the sensitivity of the results for different wave periods is examined while upper and lower limits of H_0/L_0 and θ_0 are taken as constants. During this test, since the T value is changing for distinct runs, different domains are used for each specific run to be able to include the shallow water region. Therefore, the error values for different wave periods may be thought to be partially domain-dependent. Nonetheless, the test results show the performance of the model for different T values.

Table 4.4 illustrates the RMSE change for wave angle and surf zone wave height. No plots are drawn here since the error values for different runs show no significant change in general. The "x" sign appearing under the "Wave height RMSE (m)" indicates that either no breaking occurs with these parameters or the wave height values come out to be unrealistic due to high input parameters (so no error values can be calculated). All the error results for different runs are in acceptable ranges. This makes the model applicable to a variety of wave periods. Wave angle predictions for different wave periods become more erratic when $\theta_0 = 89°$ because of the deep water wave angle input being such a high value. Lastly for this test, RBF failed to model the refraction only for the case of $T = 4$; $H_0/L_0 = 0.01$; and $\theta_0 = 89°$. Table 4.5, shows the results of the third sensitivity test. In this test, the wave period and the deep water wave angle are held constant to investigate the effects of wave steepness - from 0.01 to 0.142 with a 0.01 increment - on the model results. Indeed, the change in accuracy of refraction estimates are not dealt with since divergent wave steepness values do not alter the wave angles. Therefore, only the inner model, which is for the surf zone wave heights, is considered in this last test. In Table 4.5 no plot is drawn for $T = 12\text{s}$; $\theta_0 = 10°$ case, because breaking occurs for only three lowest H_0/L_0 values. From all the plots, it can be observed that a sharp increase in the error values occurs for some value of wave steepness. These sharp increases, which violate the ongoing trend, are hard to explain but possibly, it may be something about the nature of the analytical equations for these specific values. All the remaining error values are virtually the same. The sudden increase seems to be much higher in the case of $T = 12$.

Table 4.4. Wave angle and surf zone wave height RMSE for different wave periods.

H0/L0	0.142			0.01			Theta0 (deg)
	T	Wave angle RMSE (deg)	Wave height RMSE (m)	T	Wave angle RMSE (deg)	Wave height RMSE (m)	
	2	0.0280	x	2	0.0280	0.0000	10
	4	0.0030	x	4	0.0030	0.0044	
	6	0.0229	x	6	0.0064	0.0155	
	8	0.0371	x	8	0.0013	0.0044	
	10	0.0114	x	10	0.0113	0.0227	
	12	0.0101	x	12	0.0101	0.0353	
	T	Wave angle RMSE (deg)	Wave height RMSE (m)	T	Wave angle RMSE (deg)	Wave height RMSE (m)	89
	2	0.1381	0.0003	2	0.1970	x	
	4	0.0495	0.0045	4	RBF fails	x	
	6	0.0098	0.0115	6	0.0487	0.0016	
	8	0.0071	0.0324	8	0.0139	0.0034	
	10	0.1914	0.0662	10	0.0110	0.0058	
	12	0.1225	0.1187	12	0.0092	0.0114	

Table 4.5. Surf zone wave height RMSE change due to change in wave steepness.

T	2	12	Theta0 (deg)
	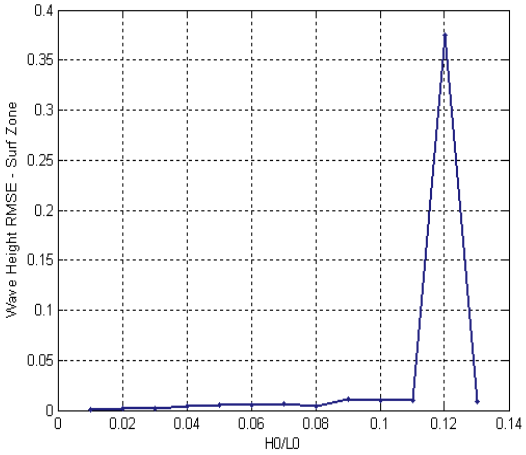	H0/L0 | Surf zone wave height RMSE 0.01 | 0.0354 0.02 | 2.4862 0.03 | 0.0463 0.04 - 0.14 | x	10
	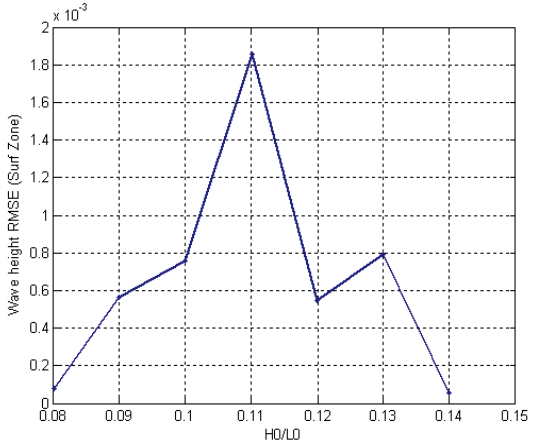	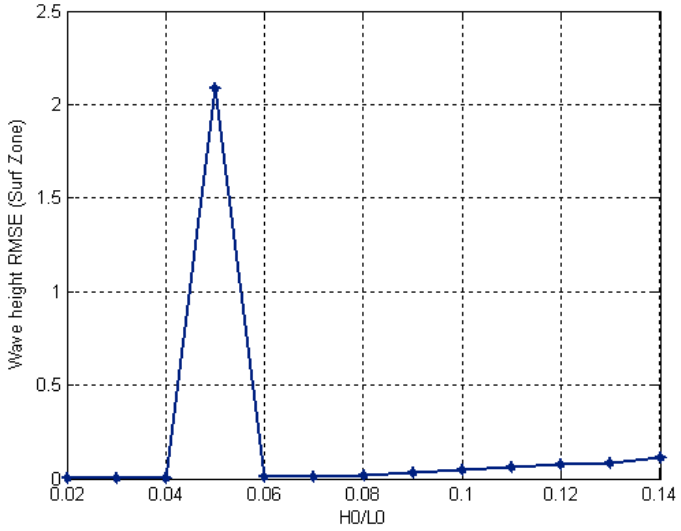	89

Since the model for the surf zone differs from the outer model, numerical results for this case are shown separately. Since the wave angles have already been computed, only the wave heights in the surf zone need to be computed. To test the model, 50 points in the onshore direction and 10 points in the longshore direction are used in the surf zone. The model works really well within the same contour that the highest variation for any contour does not exceed 6.14×10^{-3} %. Figure 4.5 includes the longshore variation of wave height for 13 equally spaced contours among the 50 contours since it would be troublesome to include all the 50 contours here. These 13 contours can serve as a representative because they are not chosen locally. The upper most from the left is the breaker-line and the lower- left is the shoreward contour. Except some slight deviations (the highest deviation is mentioned above) for a few contours, all the longshore lines for numerical results are horizontal, implying a remarkably accurate estimate of the parameter.

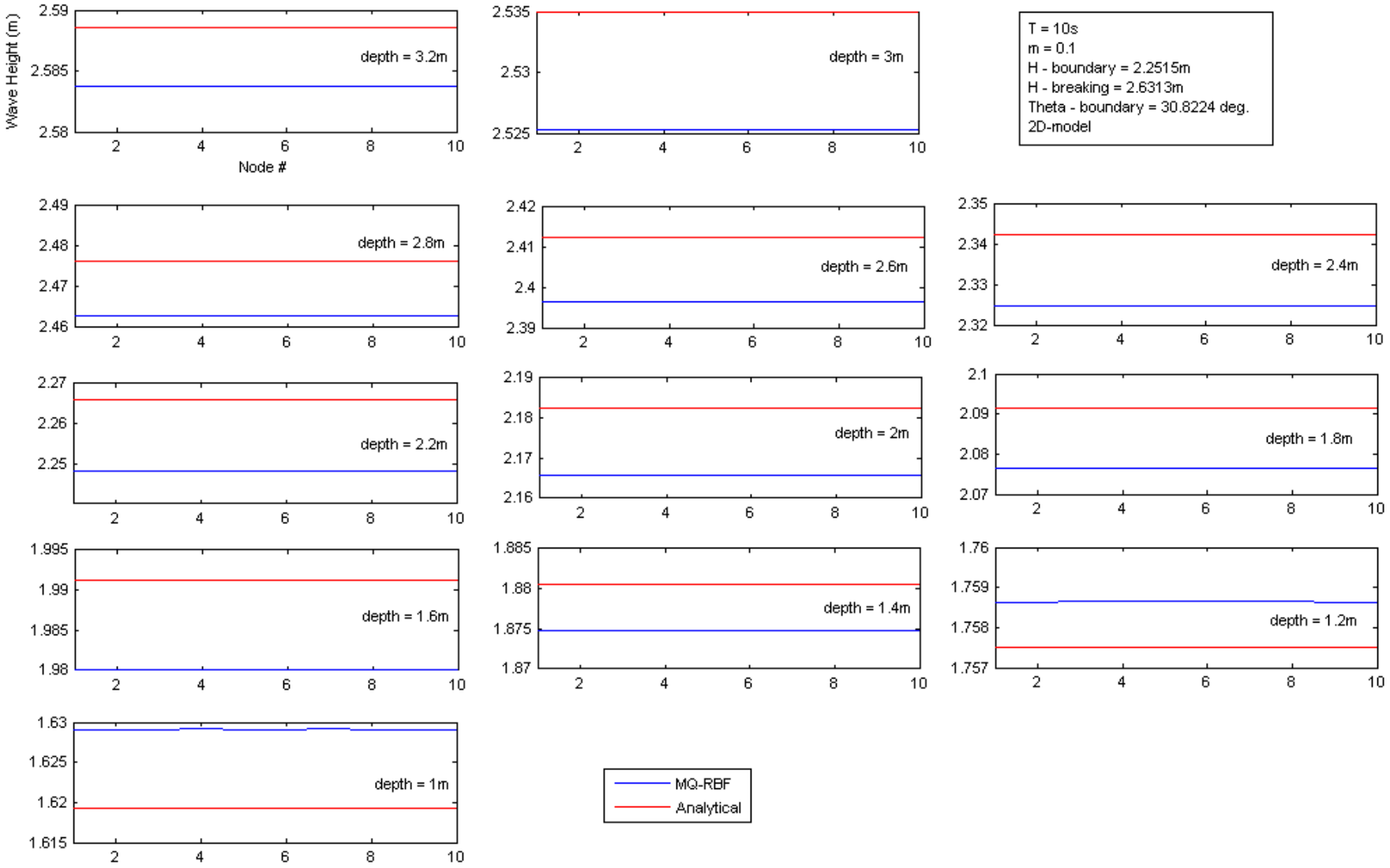

Figure 4.5. Longshore variation in wave height values, for different depth contours within surf zone.

Table 4.6. Verification of numerical surf zone wave heights.

Depth (m)	H -analytical (m)	H -numerical (m)	abs-err (m)	% err
3.3	2.6136	2.6115	0.0022	0.0824
3.2	2.5886	2.5837	0.0049	0.1889
3.1	2.5624	2.5550	0.0074	0.2882
3	2.5350	2.5253	0.0096	0.3797
2.9	2.5063	2.4947	0.0116	0.4631
2.8	2.4763	2.4630	0.0133	0.5383
2.7	2.4450	2.4302	0.0148	0.6049
2.6	2.4122	2.3962	0.0160	0.6627
2.5	2.3780	2.3611	0.0169	0.7110
2.4	2.3423	2.3248	0.0176	0.7493
2.3	2.3050	2.2871	0.0179	0.7767
2.2	2.2660	2.2481	0.0180	0.7922
2.1	2.2253	2.2076	0.0177	0.7945
2	2.1827	2.1656	0.0171	0.7823
1.9	2.1381	2.1220	0.0161	0.7540
1.8	2.0914	2.0766	0.0148	0.7078
1.7	2.0425	2.0294	0.0131	0.6420
1.6	1.9912	1.9801	0.0110	0.5546
1.5	1.9373	1.9287	0.0086	0.4433
1.4	1.8805	1.8748	0.0057	0.3055
1.3	1.8207	1.8182	0.0025	0.1377
1.2	1.7575	1.7586	0.0011	-0.0648
1.1	1.6905	1.6957	0.0052	-0.3094
1	1.6193	1.6291	0.0098	-0.6078

$y = 0$ - onshore transect is used to detail numerical wave height results moving towards shoreline. Table 4.6 includes 24 illustrative nodes for the wave heights, among the total of 50 nodes onshore. These 50 nodes are very close to each other. Because of this proximity and of the difficulty in showing all the 50 nodes here, 24 equally placed, non-local nodes are used as a representative. Computed wave heights are compared with the analytical ones. Figure 4.6 demonstrates graphically how the model results fit the exact values. Here a one-dimensional plot is used to observe the shoaling process, since the longshore variation of wave height values are dealt previously. From the figure, it is observed that surf zone model does a better job near the boundaries instead of the internal nodes.

Figure 4.7 shows the combination of both the refraction and surf zone models. The length of the arrows are proportional to wave heights. Wave height values reach their highest values between 60 – 80 meters where the breaking occurs. Thereafter, the wave heights decrease up to shoreline. This process can easily be observed from the change in the vector lengths.

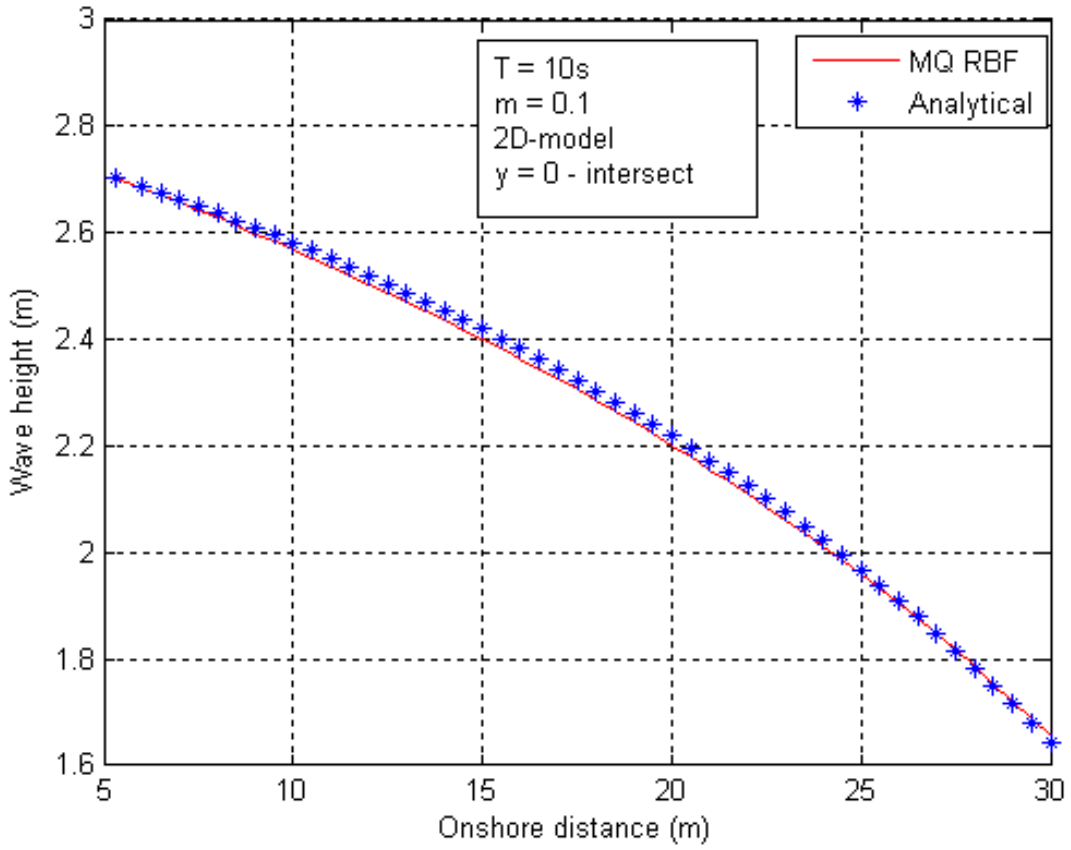

Figure 4.6. Surf zone wave decay, analytical vs. numerical results.

Apart from the verifications given above, a direct comparison between the numerical RBF model and REFDIF-1 is also performed. REFDIF-1 is typically used with monochromatic wave trains propagating in one given direction. Therefore, it would be appropriate to use REFDIF-1 to examine whether the model developed here can be as efficient as the ones that are widely used. The parameters used for the current test are the same as before. Again 10 nodes onshore are used in our numerical model and 100 nodes onshore are used in REFDIF. So, the computational grid for the RBF model is 10×10 while a 100×100 grid is used with REFDIF.

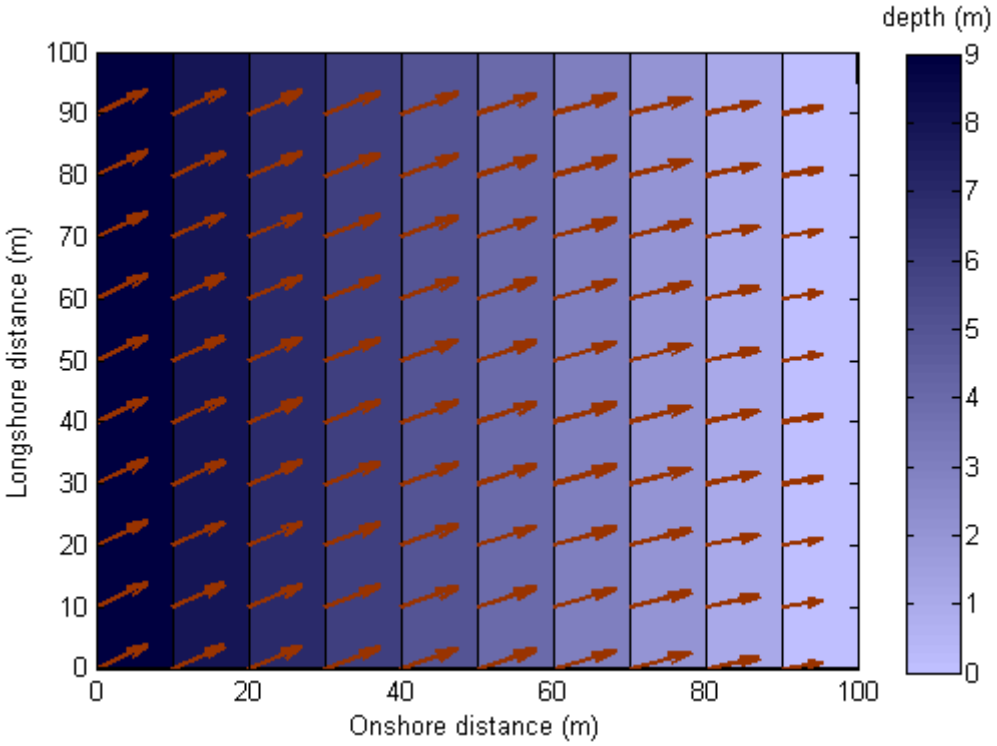

Figure 4.7. Wave height and angle variation towards shore.

Table 4.7 compares the results for the two models for the onshore transect of $y = 0$. This one-dimensional comparison suffices since the results for the same contour are shown previously to be very close to each other. Although it uses a smaller number of nodes, the RBF model results are very close to those given by REFDIF-1. It should be remembered that in this table, for the wave heights in the surf zone, only the results for the original nodes are included; that is the extra nodes added to improve the results are not dealt with.

Finally, a three- dimensional representation of wave height values from the offshore boundary up to shoreline is shown in Figure 4.8. A rapid wave decay can be detected after breaker line. This sharp decrease is related to the rather large bottom slope value of 0.1 used in the computations.

Table 4.7. Model results compared with REFDIF-1 output.

	WAVE HEIGHT (m)				**WAVE ANGLE** (deg.)		
Depth	**Analytical**		**RBF***	**REFDIF-1** (100x100)	**Analytical**	**RBF** (10x10)	**REFDIF-1** (100x100)
10	2.3182	Eq. 1.16	2.3182	2.3182	30.0009	30.0009	30.0000
9	2.3388		2.3382	2.3420	28.5409	28.4902	28.5381
8	2.3669		2.3665	2.3729	26.9811	26.9450	26.9819
7	2.4047		2.4045	2.4136	25.3040	25.2796	25.3061
6	2.4559		2.4558	2.4673	23.4854	23.4768	23.4899
5	2.5259		2.5259	2.5397	21.4906	21.5003	21.4917
4	2.6246		2.6248	2.6407	19.2662	19.3012	19.2761
3	2.5810	Eq. 1.28	2.5683	2.5710	16.7220	16.7922	16.7239
2	2.2184		2.2007	2.1660	13.6826	13.8172	13.6881
1	1.6433		1.6547	1.5748	9.6948	9.9787	9.7221

**(10x10 before; 50x10 after breaker line)*

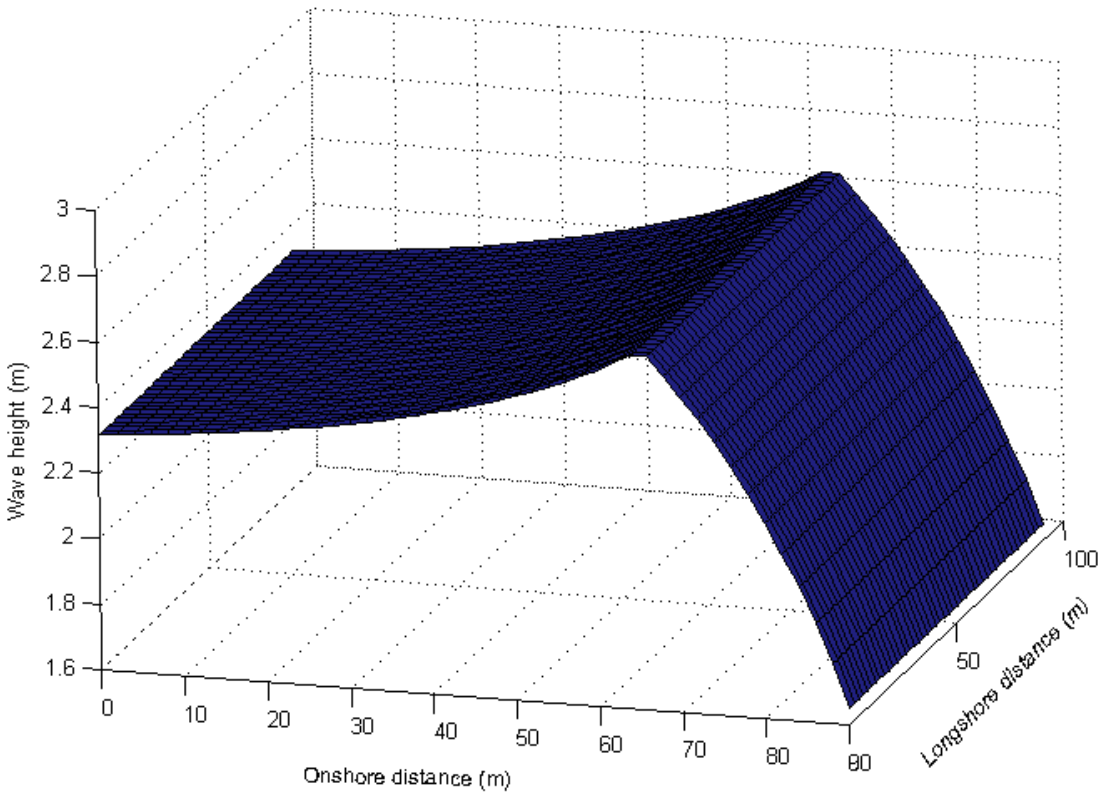

Figure 4.8. Wave height variation towards the shore over a linear bathymetry.

Apart from the tests conducted on a regular grid, a random node distribution is also tested to prove the efficiency and strength of the RBFCM in meshless cases. 100 nodes, with the furthest node being 100m and the nearest one being 1m from the shoreline, are used. The node distribution is illustrated in Figure 4.9. Again, a 0.1 bottom slope is used. Deep water wave parameters are the same as the previous regular-grid case.

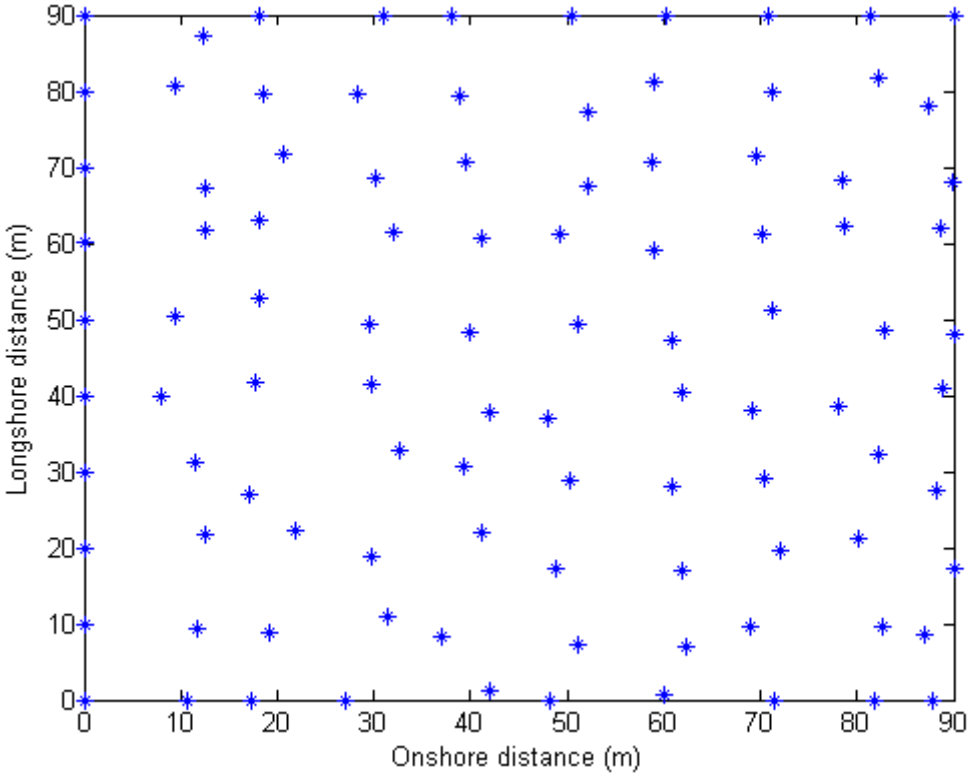

Figure 4.9. Random node distribution.

Figure 4.10 compares the computed wave angles with the analytical ones. A nice fit, which has a maximum relative error of 1.8835 %, can easily be observed. For the inner model calculations of the wave heights in the surf zone, a larger number of nodes are needed for an acceptable degree of accuracy that is with a relative error of approximately 0.20 % in average; a number reached from the previous wave angle computations. These extra nodes, which add up to a total of 520 after the breaker line, are also randomly located. Figure 4.11 shows the distribution of the nodes both before and after the breaker line. The red dots are the original nodes and the green ones are the extra nodes used in the surf zone region. Figure 4.12 shows the perfect agreement, which has an average relative error of 0.1392 %, achieved between the analytical and numerical results for the wave heights in the surf zone. The comparison of analytical and numerical wave heights between the offshore boundary and the shore is shown in Figure 4.13.

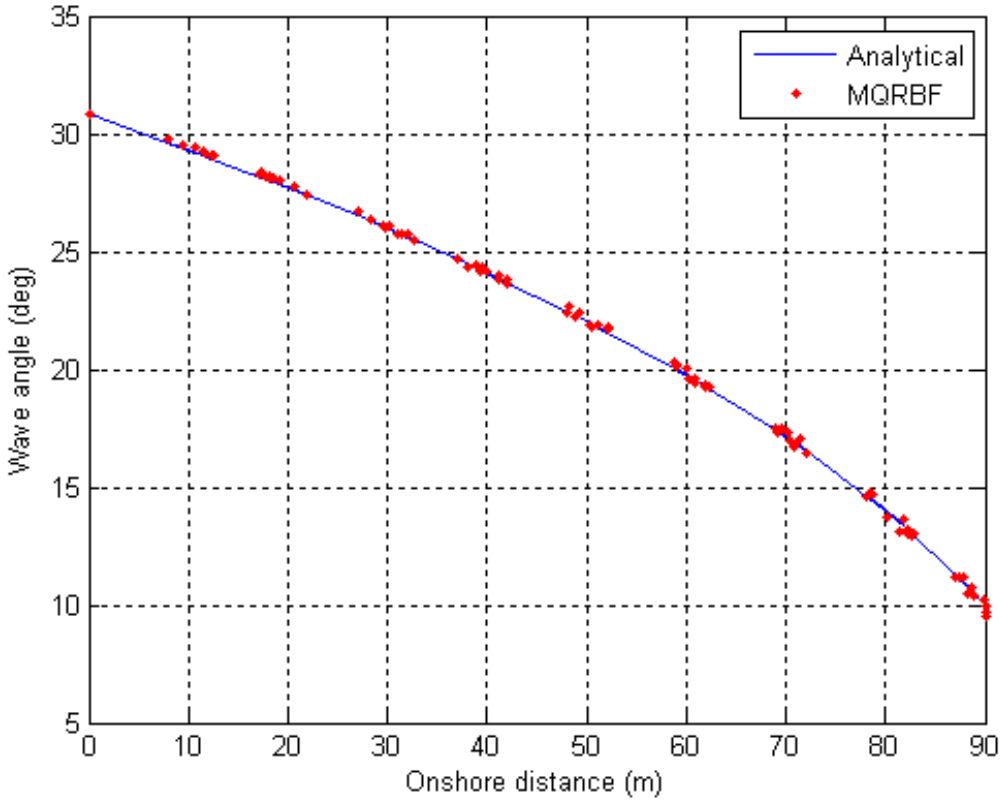

Figure 4.10. Wave refraction; analytical vs. numerical results: Meshless case.

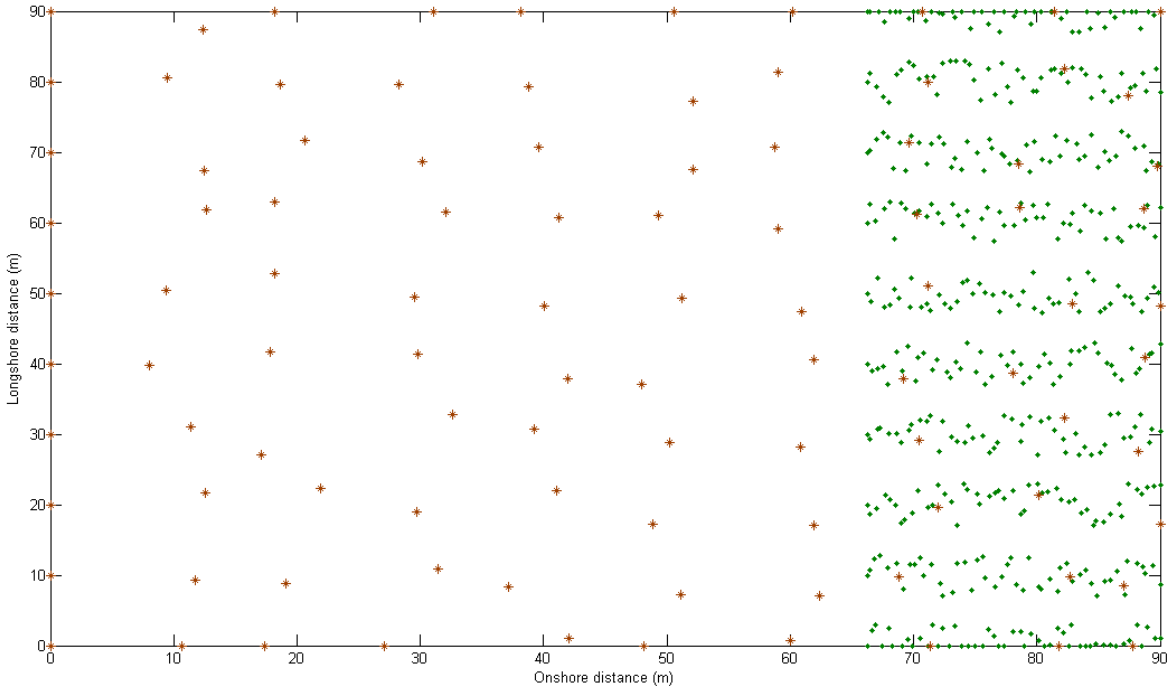

Figure 4.11. Node placement in the surf zone: Meshless case.

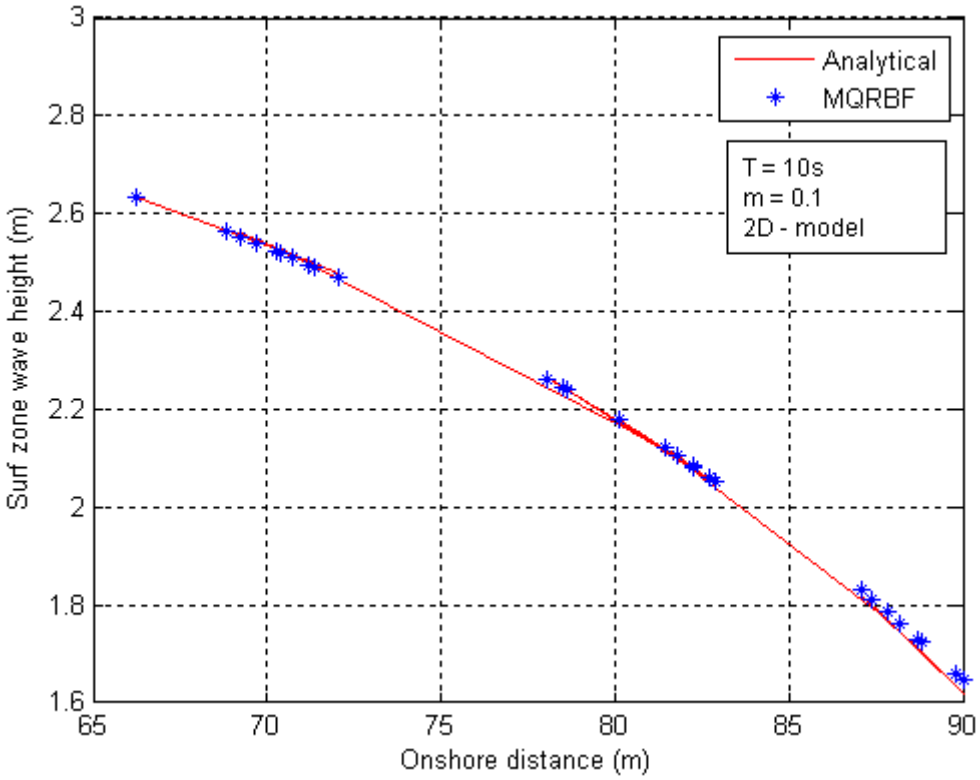

Figure 4.12. Surf zone wave heights, analytical vs. numerical: Meshless case.

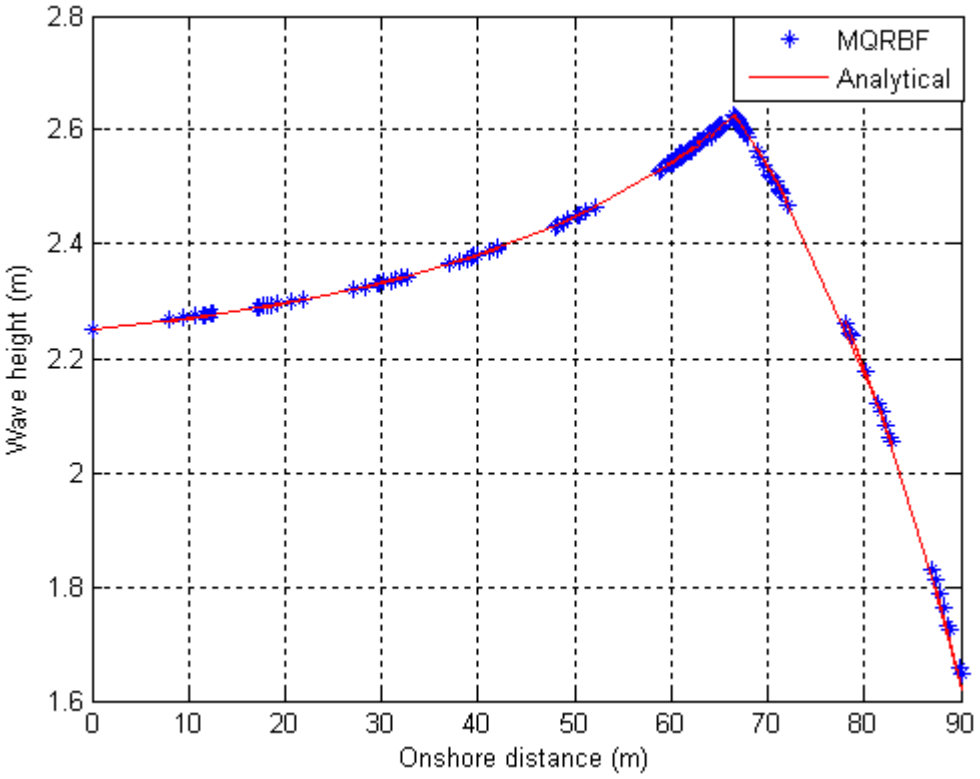

Figure 4.13. Wave heights over the computational region: Meshless case.

4.2. Variable Bottom Topography

The second phase of the model verification studies was carried out using Noda (1974)'s analytical bathymetry expressions given previously in the problem definition section. During the numerical tests conducted in this latter part of the study, three different longshore periodic bottom profiles are applied. First of these profiles is the sinusoidal beach topography. It should be kept in mind that the shape of the shoreline is the same of the bottom contour. For the first case, a beach slope of 0.03, and a computational grid of 50×50 is used. The grid size is larger than the plane bottom case because here we have a milder beach, which makes necessary to start the computations further offshore to observe the shoaling and breaking processes. Therefore, problem boundary locates at 500 meters offshore. The parameters used in Noda (1974)'s sinusoidal function are: $a = 10$, $\lambda = 100$. The wave period was taken as 10s. Deep water wave parameters are the same as before: $\theta_0 = 60^{\circ}$ and $H_0 = 3$m. Figure 4.14 shows the wave refraction over a sinusoidal bathymetry. The computational domain starts in intermediate water where the bottom begins to affect the wave behavior and parameters. It can be seen from the figure that wave refraction occurs within this region but it becomes more pronounced after $x > 350$ meters onshore, where the shallow- water zone begins. The model does behave just as the way we expect it to behave; the wave is refracted and bent towards shallower regions of the bathymetry. The same problem, with the same parameters, was also solved using REFDIF-1. The same computational grid, 50×50, was used. The RBF model developed in this study is based on linear wave theory. However, REFDIF uses a different analytical scheme, a weakly nonlinear one, to model the wave parameters. REFDIF also contains diffraction which causes a convergence or divergence of wave energy that influences wave refraction and shoaling processes. Diffraction is not included in this work. Therefore, we do not anticipate a strong similarity between the outputs of the two numerical models. However, there should be considerable similarity in mainlines of the refraction pattern. The REFDIF results are plotted in Figure 4.15. The REFDIF results exhibits a slower response to depth change in both of the directions than the RBF model results. Wave refraction is less pronounced in intermediate water. In order to explore whether the model behaves the same for the symmetrical regions in the bathymetry, we let the offshore boundary wave angle to be 0°. Figure 4.16 shows the RBF results for the refraction pattern over a sinusoidal bottom. The refraction of the waves can be clearly observed especially in

shallow water. The corresponding REFDIF results are given in Figure 4.17. Refraction begins at $x = 450$ meters onshore. Lastly, wave heights across the computational region are calculated and plotted in Figure 4.18 and Figure 4.19. It should be noted that since the surf zone region requires more nodes for an acceptable accuracy (with an average relative error approximately less than 1 %), here again the number of nodes is increased after the breaker line. However, because of the gently sloping beach, breaking occurs far from the shoreline. This results in a matrix with a huge number of entries, making the computation impossible with my personal computer. Hence, for these varying bottom topographies analytical results are used for the wave heights within the surf zone.

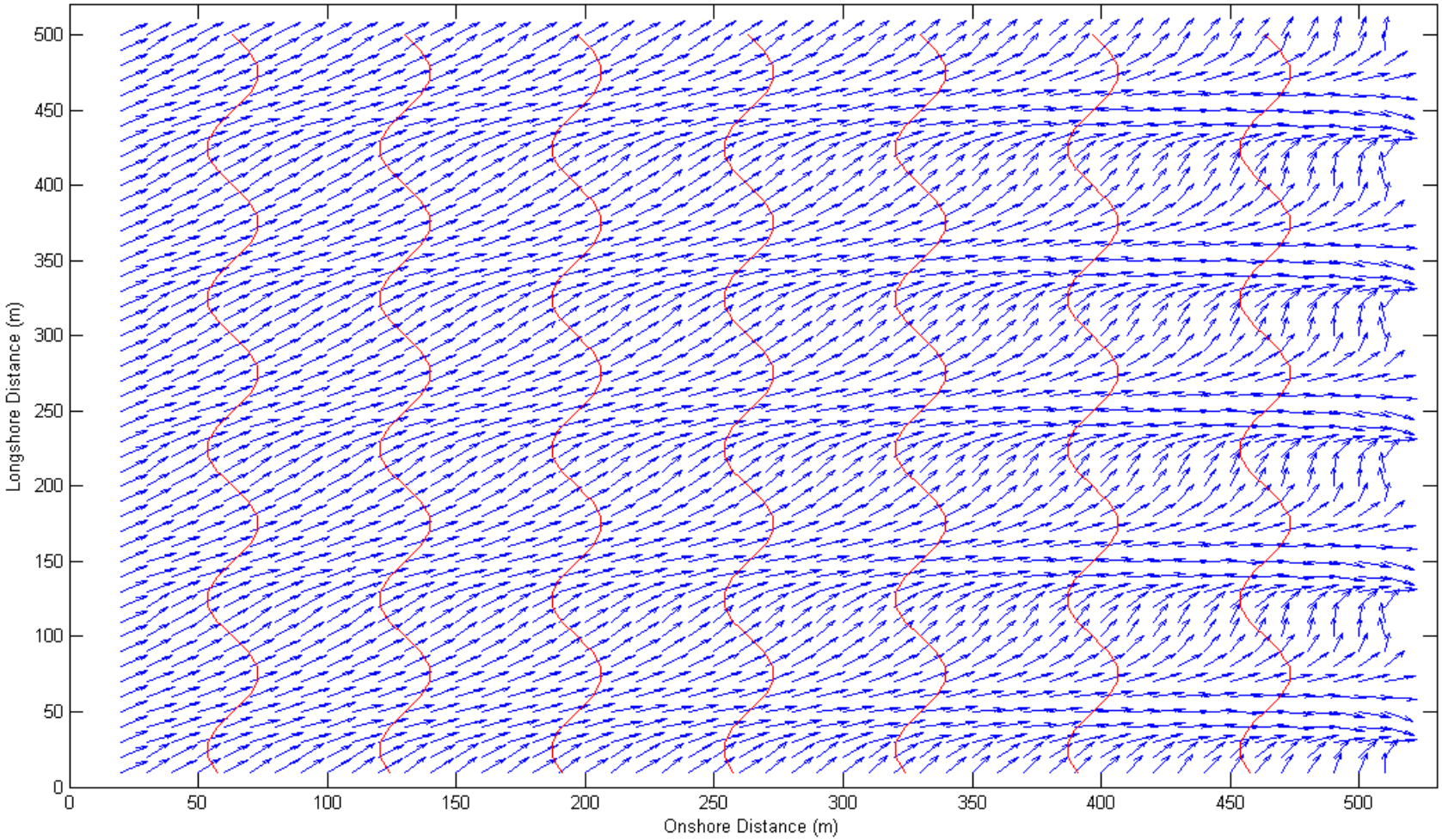

Figure 4.14. Wave refraction over sinusoidal bathymetry; RBF case.

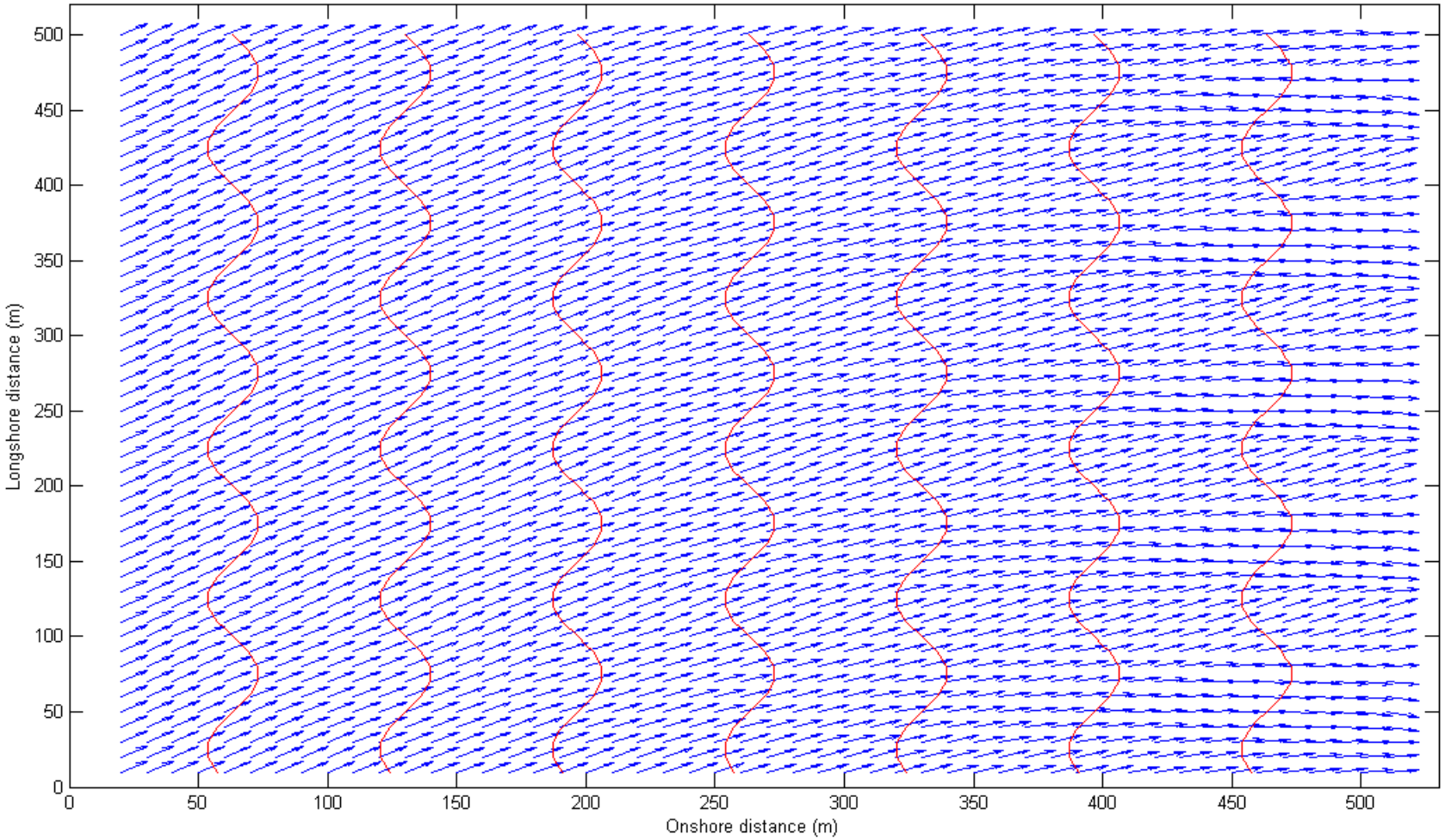

Figure 4.15. Wave refraction over sinusoidal bathymetry, REFDIF-1 output.

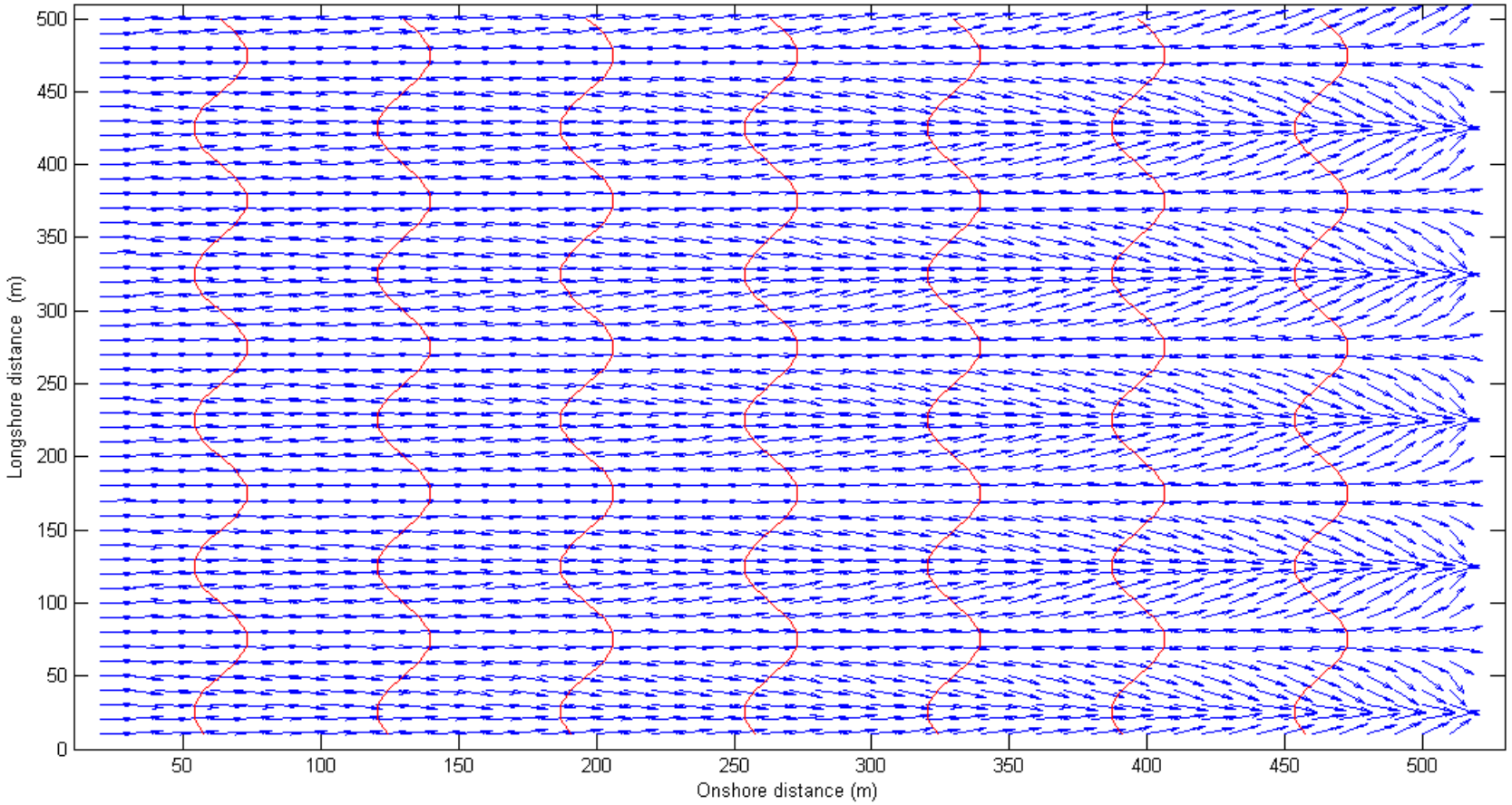

Figure 4.16. RBF refraction results for the case of offshore boundary = 0°.

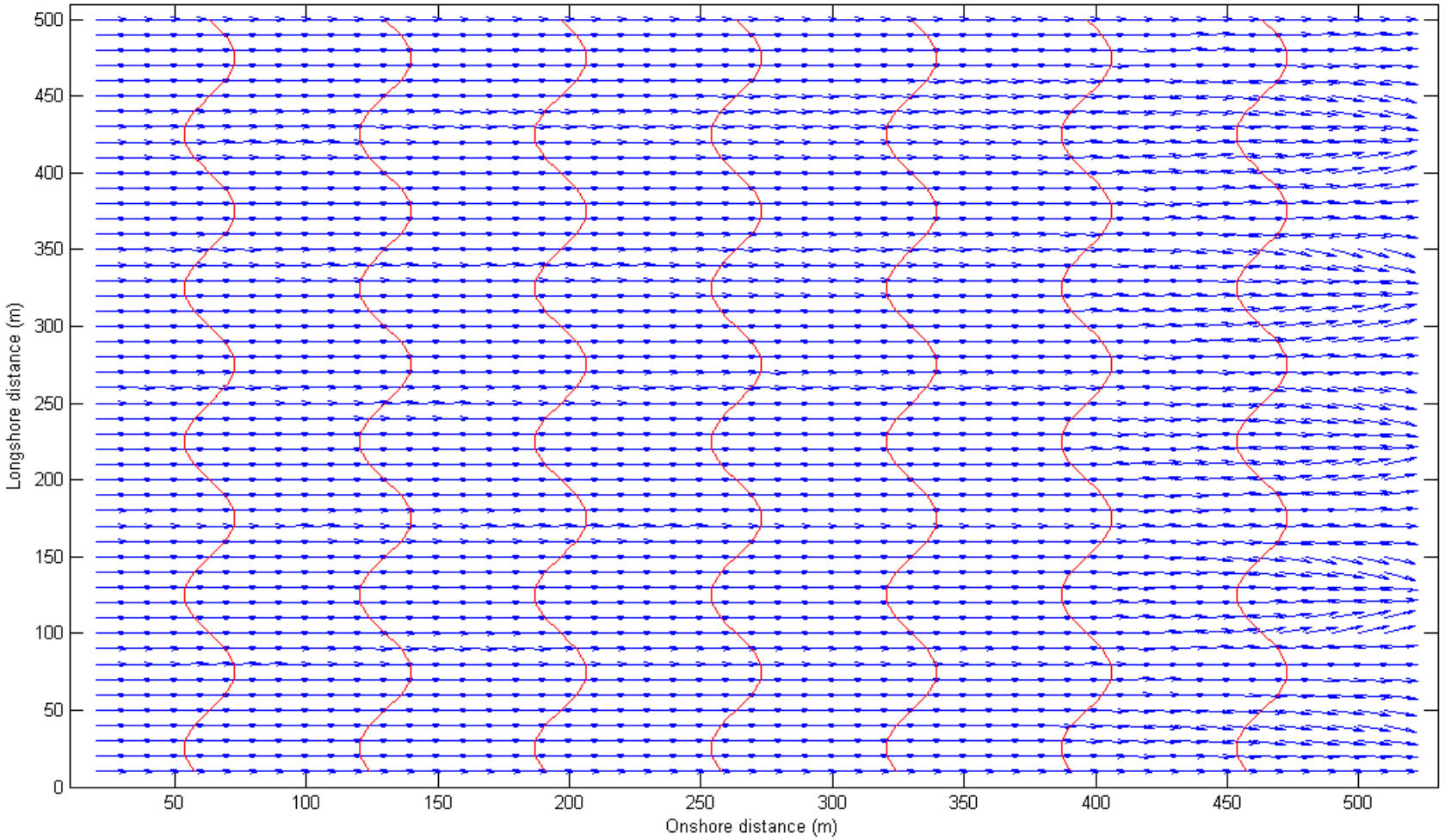

Figure 4.17. Wave refraction in the case of offshore boundary = 0°; REFDIF-1 output.

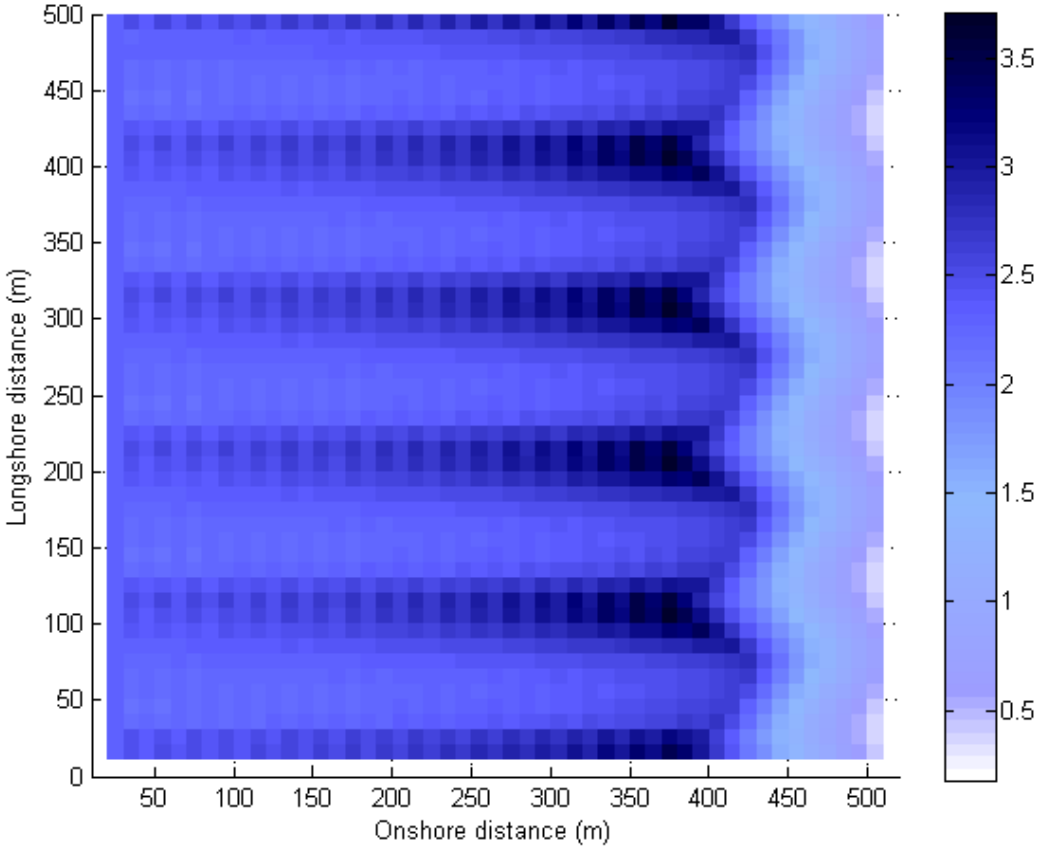

Figure 4.18. Wave height variation on sinusoidal bathymetry, RBF results.

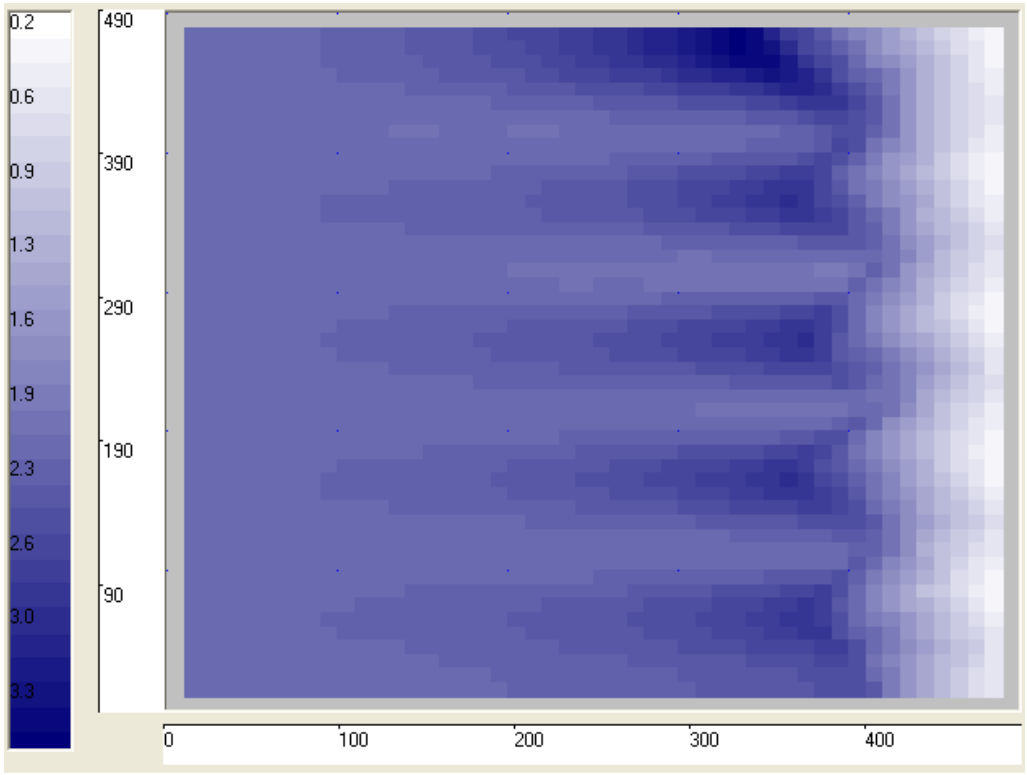

Figure 4.19. Wave height variation on sinusoidal bathymetry, REFDIF-1 output.

Besides the sinusoidal bottom case, periodic bottom, and periodic bottom with skewed channel topographies are also tested. All the wave parameters are the same except for the bottom slope that is taken to be $m = 0.025$ for these topographies. The parameters used in Noda (1974)'s periodic bottom function are: $a = 10;\ \ b = 3/10^{1/3};\ \ \lambda = 200.$ Periodic bottom with skewed channel is also created with the same functional parameters. Differently, an angle-related parameter is also included in the description of this last function. A value of $\alpha_s = 30°$ is defined for this angle in this study. Wave refraction pattern for the periodic bottom is shown in Figure 4.20 and Figure 4.21 for RBF and REFDIF, respectively. Same conclusions drawn for the sinusoidal case hold for the periodic bottom as well. Again, the smoothing character of the diffraction included in REFDIF model can be observed. Figure 4.22 and Figure 4.23 follow; representing the wave heights for the related bottom. Lastly, numerical wave refraction for the periodic bottom with skewed channel topography is demonstrated in Figure 4.24. Up to very nearshore it is hard to track the refraction process because of the skewness included. Similar results are obtained from the associated REFDIF run and the output is graphed in Figure 4.25. Finally, Figure 4.26 and Figure 4.27 contain the wave height variation across periodic beach with skewed channel, for the RBF and REFDIF cases, respectively.

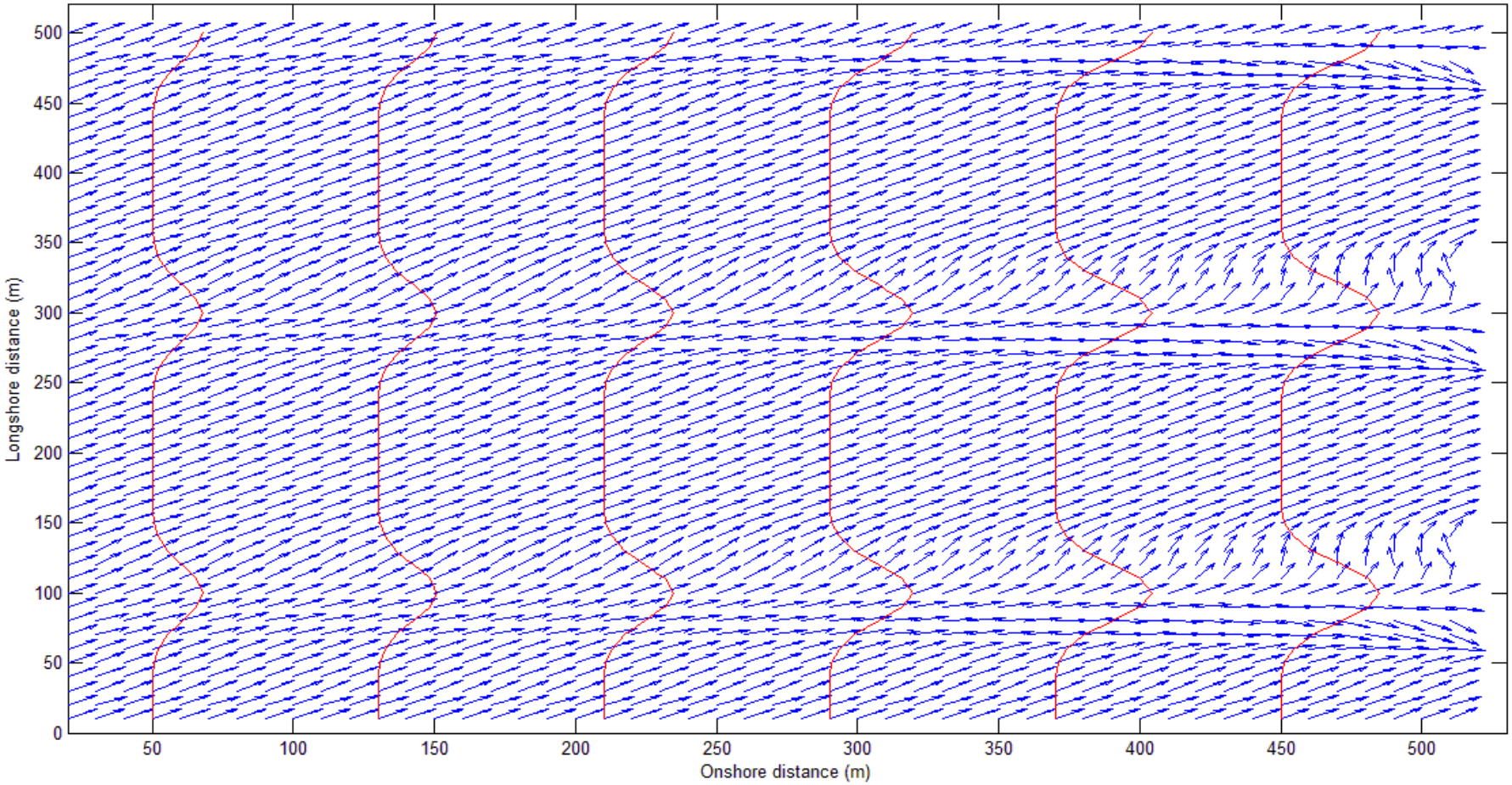

Figure 4.20. Wave refraction over periodic bottom profile, RBF results.

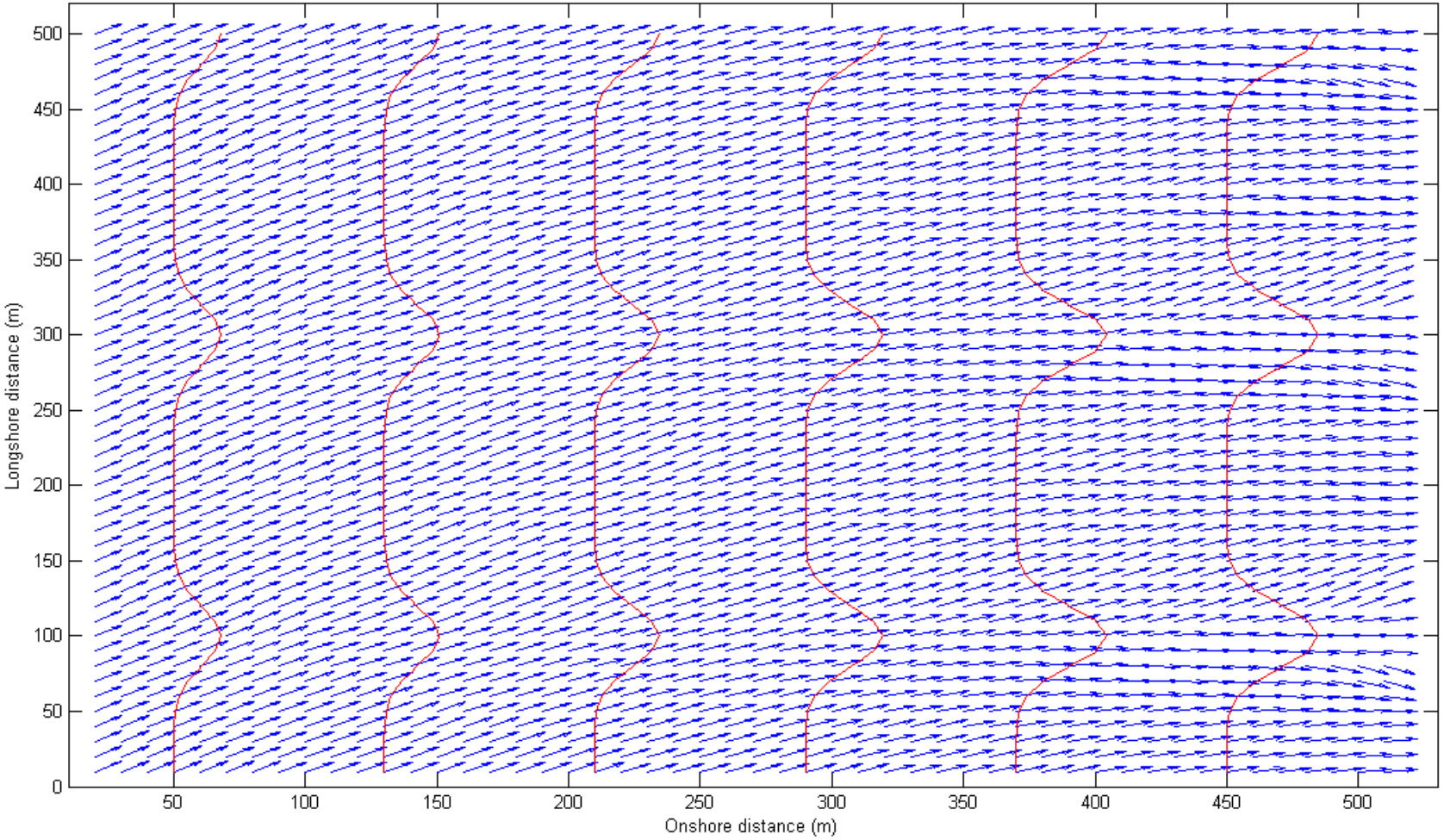

Figure 4.21. Wave refraction over periodic bottom profile, REFDIF-1 output.

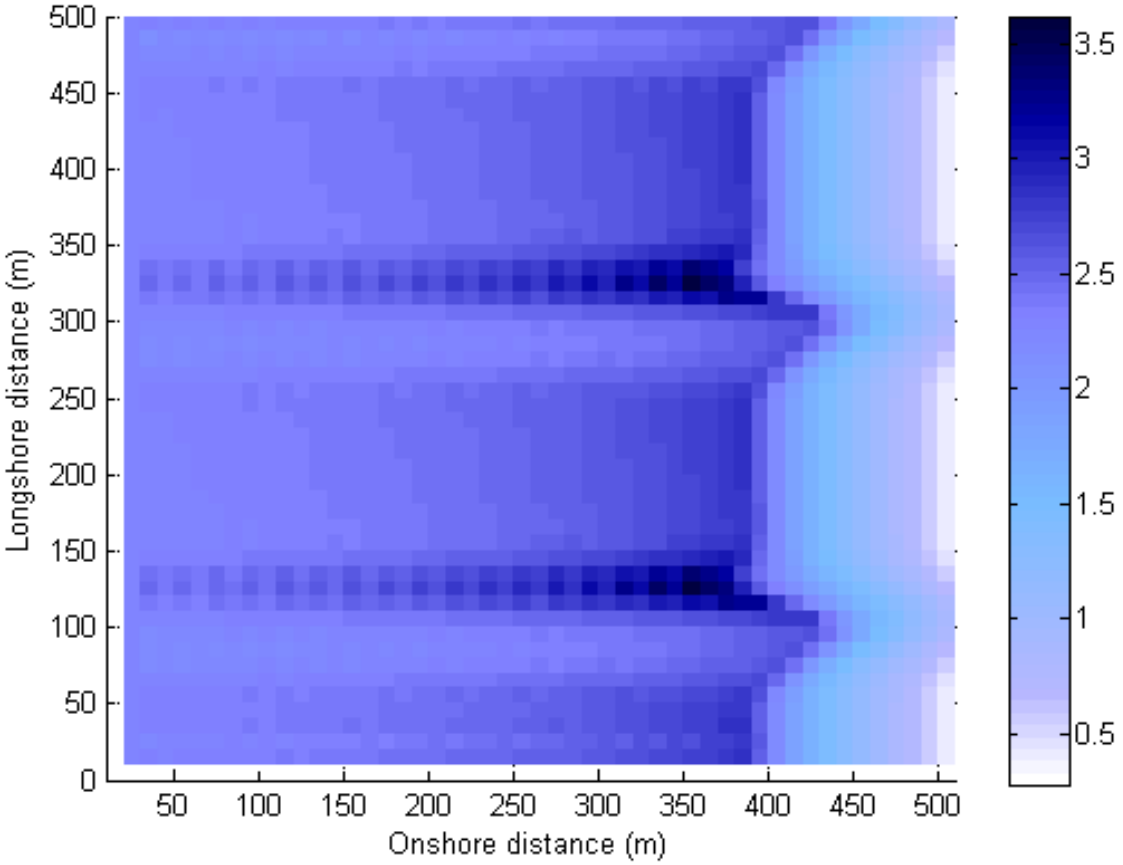

Figure 4.22. Wave height variation on periodic bottom profile, RBF results.

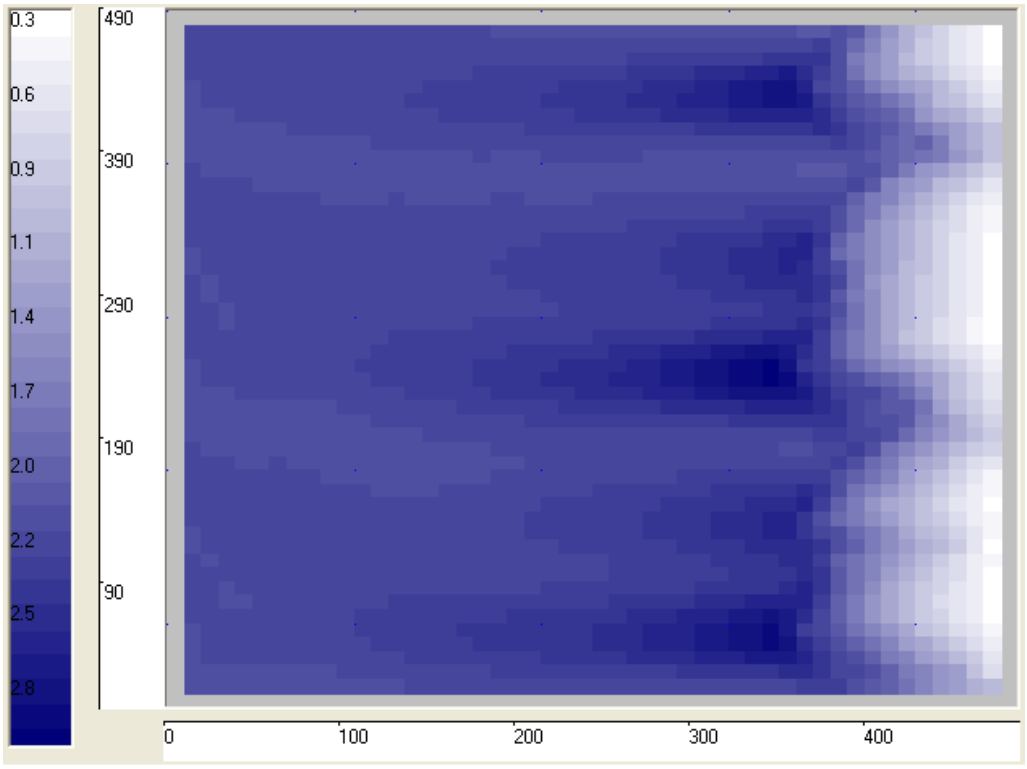

Figure 4.23. Wave height variation on periodic bottom profile, REFDIF-1 output.

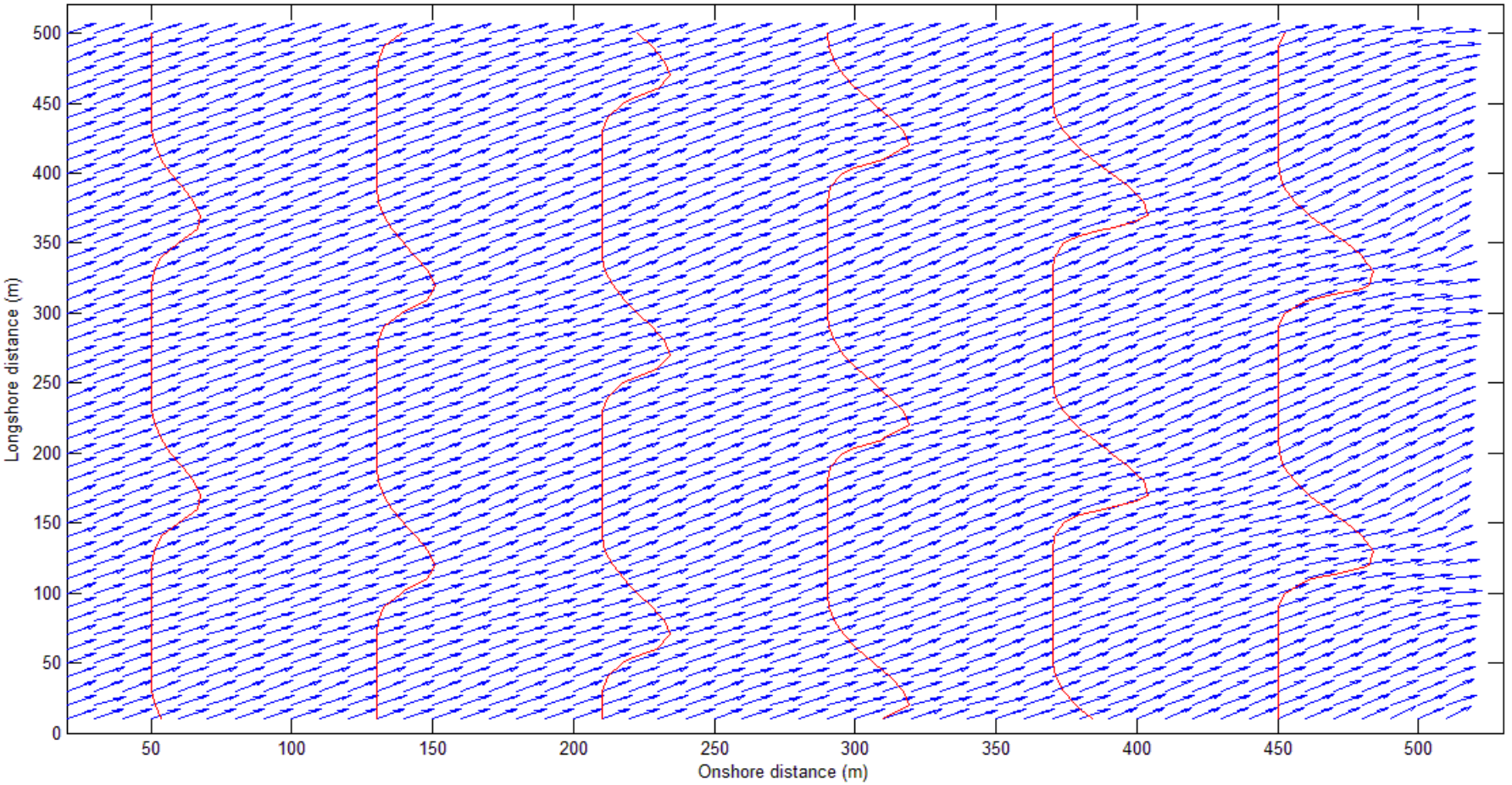

Figure 4.24. Wave refraction over periodic bottom profile with skewed channel, RBF results.

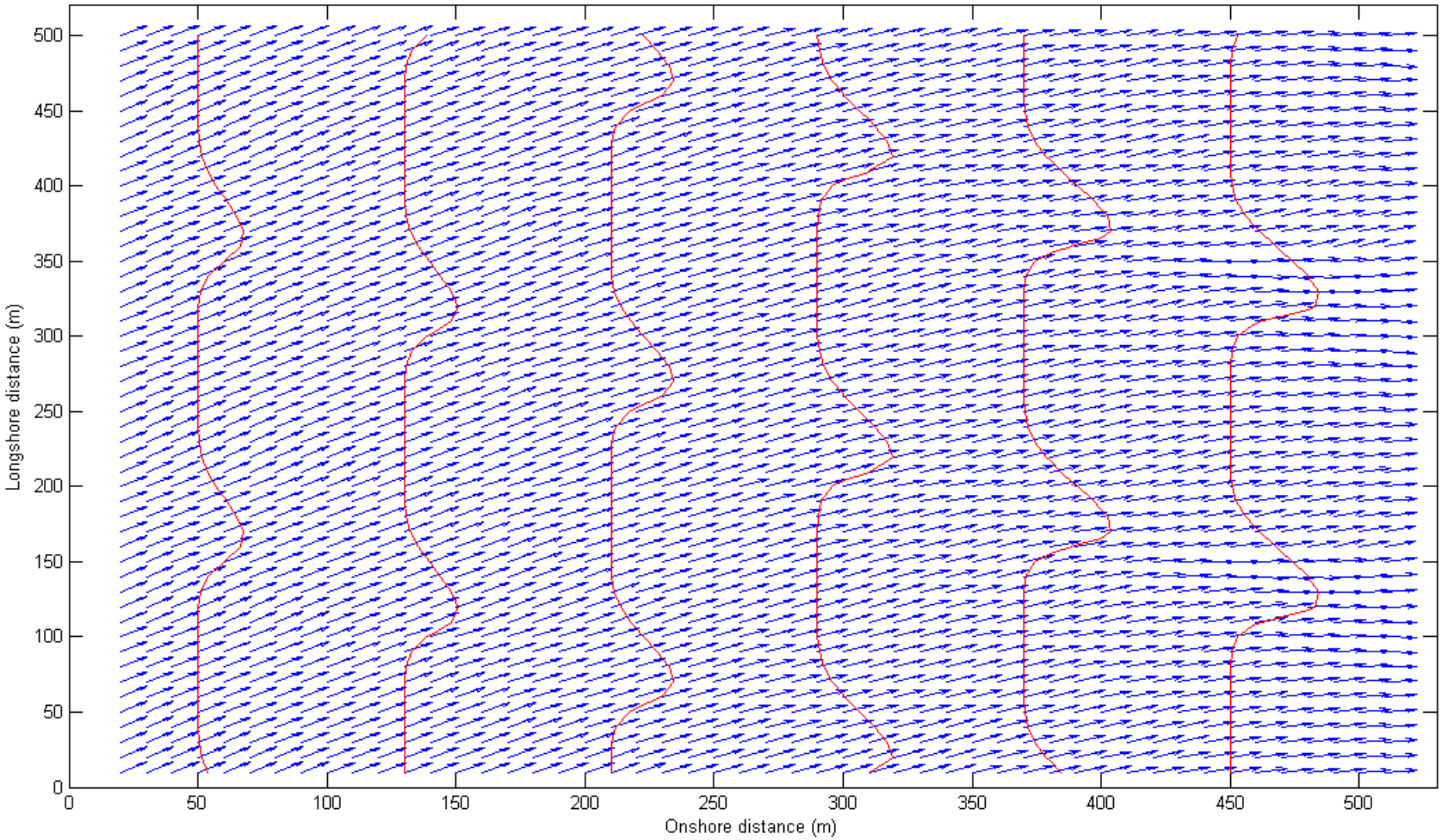

Figure 4.25. Wave refraction over periodic bathymetry with skewed channel, REFDIF-1 output.

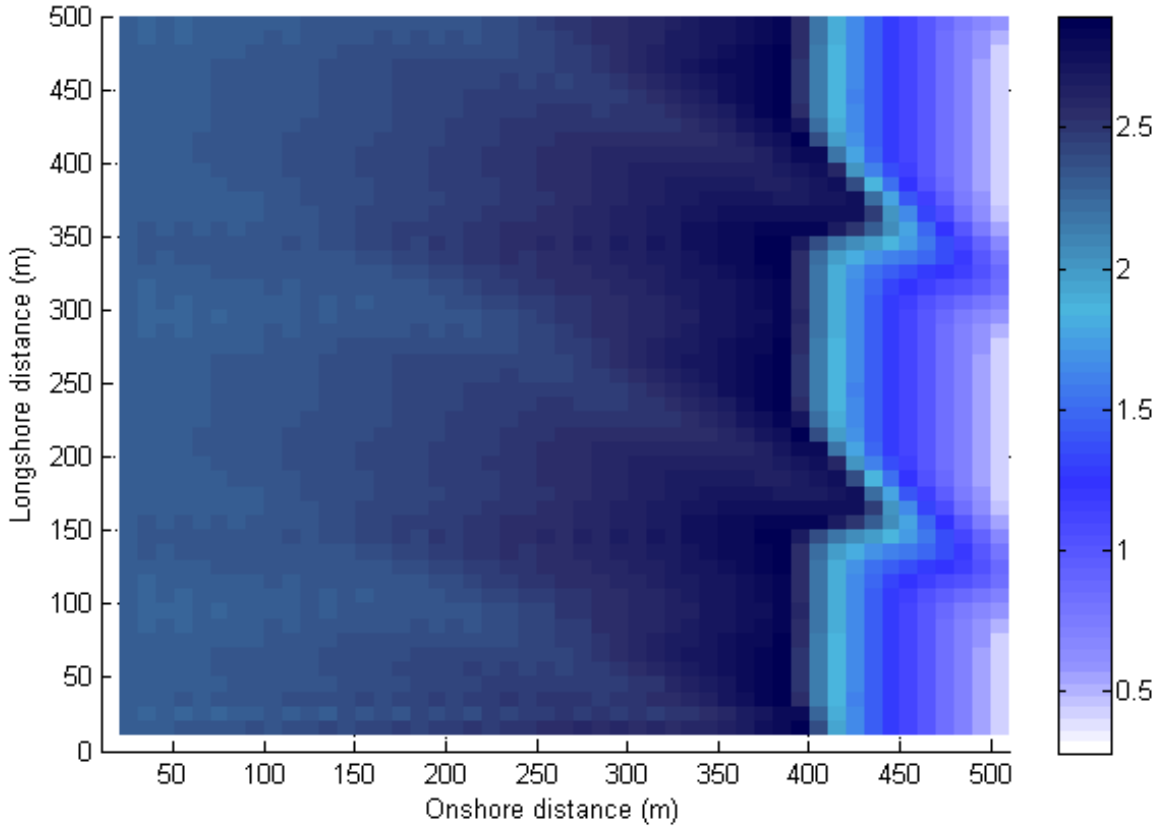

Figure 4.26. Wave height variation on periodic bottom with skewed channel, RBF results.

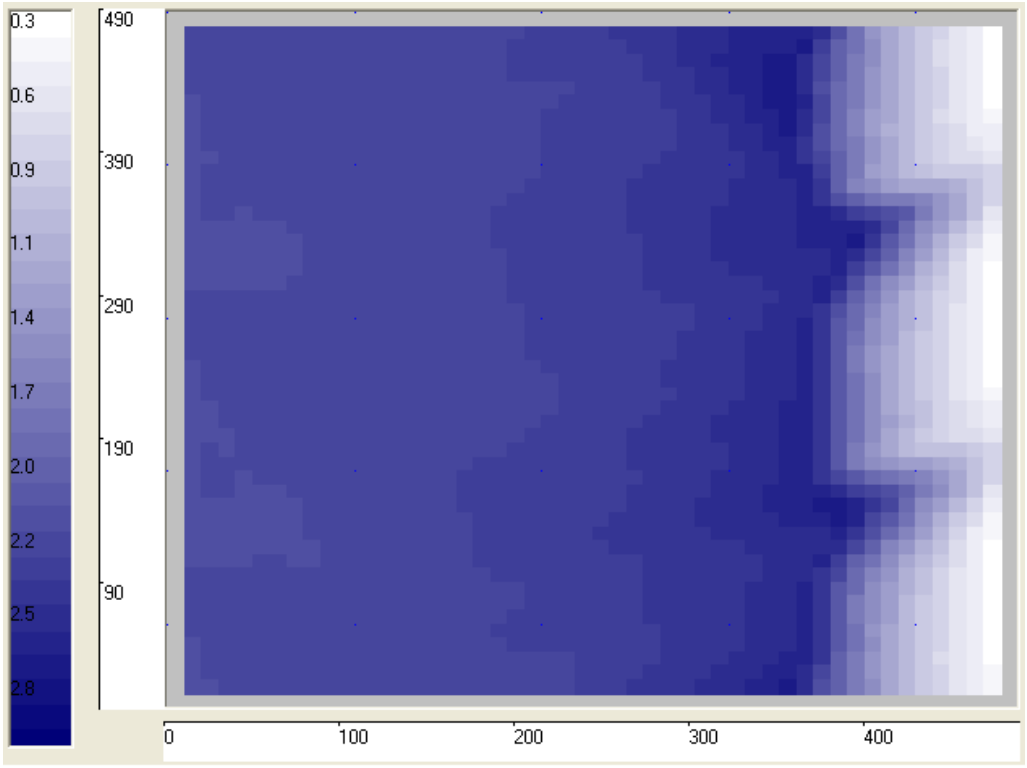

Figure 4.27. Wave height variation on periodic bottom with skewed channel, REFDIF-1.

5. CONCLUSIONS AND RECOMMENDATIONS

An MQRBF numerical model of nearshore wave transformation has been developed that incorporates the refraction, shoaling, breaking and re-forming processes to produce the local wave angles and wave heights. The model is initially tested for a plane bottom, where the analytical solutions are available. It yields favorable results when they are quantitatively compared with the exact solutions. Thus, it is proven that the RBFCM is an efficient and accurate way of solving the nearshore wave transformation problem. The model is also run for waves propagating over a variable bottom topography, and the results are compared with the corresponding REFDIF-1 outputs. The RBFCM is shown to reliably predict wave parameters for different bottom topographies.

Overall, the RBFCM is proven to be an efficient and easy-to-use numerical technique which makes it a highly advantageous method. It avoids all kinds of meshes, enabling the expenditure of much less effort than the other mesh dependent numerical methods. The implementation of the MQ method considerably lessens the computational time needed to run the related algorithm. Of course, the method has certain limitations. A disadvantage of the method is its full matrix, which normally hinders its application to large-scale problems. Fortunately, recent developments, such as domain decomposition, have shown to successfully improve the computational efficiency.

The model developed in the present study is open to some improvements. Diffraction, which is not included herein, can be incorporated to the model to be able to predict the wave parameters more reliably. Moreover, the model may also be tested for some other real bathymetries. In addition, certain improvements for the model within the surf zone can be made to improve the computational efficiency since much more nodes are needed during the determination of wave heights after breaker line.

REFERENCES

Battjes, J.A. and J.P.F.M. Janssen, 1978, "Energy Loss and Set-up due to Breaking of Random Waves", *Proceedings of the 16th International Conference on Coastal Engineering*, American Society of Civil Engineers, New York, Vol. 1, pp. 569-587.

Battjes, J.A., 1972, "Set-up due to Irregular Waves", *Proceedings of the 13th International Conference on Coastal Engineering*, American Society of Civil Engineers, New York, Vol. 3, pp. 1993-2004.

Booij, N., R. C. Ris and L. H. Holthuijsen, 1999, "A Third-Generation Wave Model for Coastal Regions, Part I: Model Description and Validation", *J. Geophys. Res*, Vol. 104, C4, pp.7649-7666.

Buhmann, M.D., 2000, "Radial Basis Functions", *Acta Numerica*, Vol. 9, pp. 1-38.

Buhmann, M.D., 2003, *Radial Basis Functions, Theory and Implementations*, Cambridge University Press, Cambridge.

Collins, J.I., 1970, "Probabilities of Breaking Wave Characteristics", *Proceedings of the 12th International Conference on Coastal Engineering*, American Society of Civil Engineers, New York, Vol. 1, pp. 339-412.

Dally, W.R., R.G. Dean and R.A. Dalrymple, 1985, "Wave Height Variation Across Beaches of Arbitrary Profile", *J. Geophys. Res.*,Vol. 90, pp. 11917-11927.

Dean, R.G. and R.A. Dalrymple, 1991, *Water Wave Mechanics for Engineers and Scientists*, World Scientific Publishing, Singapore.

Fasshauer, G.E., 2007, *Meshfree Approximation Methods with Matlab*, Interdisciplinary Mathematical Sciences- vol. 6, World Scientific Publishing, Singapore.

Goda, Y., 1975, "Irregular Wave Deformation in the Surf Zone", *Coastal Engineering Journal*, pp.13-26.

Golberg, M.A., C.S. Chen and S. Karur, 1996, "Improved Multiquadric Approximation for Partial Differential Equations", *Engineering Analysis with Boundary Elements*, Vol.18, pp. 9-17.

Hardy, R.L., 1971, "Multiquadric Equations of Topography and Other Irregular Surfaces", *Journal of Geophysical Research*, Vol. 76, pp. 1905-1915.

Hon, Y.C. and X.Z. Mao, 1997, "A Multiquadric Interpolation Method for Solving Initial Value Problems", *Sci. Comput.*, Vol. 12, pp. 51-55.

Hon, Y.C. and X.Z. Mao, 1998, "An Efficient Numerical Scheme for Burgers' Equation", *Appl. Math. Comput.*, Vol. 95, pp. 37-50.

Hon, Y.C., 1993, "Typhoon Surge in Tolo Harbour of Hong Kong – An Approach using Finite Element Method with Quadrilateral Elements and Parallel Processing Techniques", *Chinese J. Num. Math. Appl.*, Vol. 15, pp. 21-33.

Kansa, E.J. 1990a, "Multiquadrics- A Scattered Data Approximation Scheme with Applications to Computational Fluid Dynamics-I", *Computers and Mathematics with Appplications*, Vol 19, pp. 127-145.

Kansa, E.J., 1990b, "Multiquadrics- A Scattered Data Approximation Scheme with Applications to Computational Fluid Dynamics-II", *Computers and Mathematics with Appplications*, Vol 19, pp. 147-161.

Kansa, E.J., 1986, "Application of Hardy's Multiquadric Interpolation to Hydrodynamics", *Proc. 1986 Simul. Conf.*, Vol. 4, pp. 111-117.

Kirby, J.T. and R.A. Dalrymple, 1986, "Modeling Waves in Surfzones and Around Islands", *Journal of Waterway*, Port, Coastal Ocean Eng, Vol. 112, pp. 78-93.

Kuo, C.T. and S.T. Kuo, 1974, "Effect of Wave Breaking on Statistical Distribution of Wave Heights", *Proceeding of the Third Conference on Civil Engineering in the Oceans*, American Society of Civil Engineers, New York, Vol. 2, pp. 1211-1231.

Madsen, P.A. and O.R. Sorensen, 1992, "A new Form of the Boussinesq Equations with Improved Linear Dispersion Characteristics. Part-2. A Slowly Varying Bathymetry", *Coastal Eng.*, Vol. 18, pp. 183-204.

McCowan, J., 1894, "On the Highest Wave of Permanent Type", *Philos. Mag. J. Sci.*, Vol. 38, pp. 351-358.

Michelli, C.A.,1986, "Interpolation of Scattered Data: Distance Matrices and Conditionally Positive Definite Functions", *Constr. Approx,* Vol. 2, pp. 11-22.

Noda, E.K., 1974, "Wave - Induced Nearshore Circulation", *Journal of Geophysical Research*, Vol. 79, pp. 4097-4106.

Ris, R. C., L. H. Holthuijsen, and N. Booij, 1999, "A Third-Generation Wave Model for Coastal Regions, Part II: Verification", *J. Geophys. Res*. Vol. 104, C4, pp.7667-7681.

Schaback, R. and Y.C. Hon, 2001, "On Unsymmetric Collocation by Radial Basis Functions", *Journal of Applied Mathematics and Computation*, Vol. 119, pp. 177-186.

Svendsen, I. A., 1984, "Wave Heights and Set-up in a Surf Zone", *Coast. Eng.*, Vol. 8., pp. 303-329.

Thornton, E.B. and R.T. Guza, 1983, "Transformation of Wave Height Distribution", *J. Geophys. Res.*,Vol. 88, pp. 5925-5938.

Wendland, H., 2005, *Scattered Data Approximation*, Cambridge University Press, Cambridge.

Wornom, S. F., D. J. S Welsh and K. W. Bedford, 2001, “On Coupling the SWAN and WAM Wave Models for Accurate Nearshore Wave Predictions”, *Coastal Engineering Journal*, Vol. 43, No. 3, pp.161-201.

REFERENCES NOT CITED

Andrew, C. J. F., *Bibliographical Review of Nearshore Wave Models*, DSTO Aeronautical and Maritime Research Laboratory, Melbourne, Australia, 1999.

Chen, C.S., Y.C. Hon and R.A. Schaback, *Scientific Computing with Radial Basis Functions*, Manuscript, 2007.

Kirby, J.T. and R.A. Dalrymple, *REF/DIF 1 Documentation and User's Manual*, Center for Applied Coastal Research Department of Civil Engineering, University of Delaware, Newark, 1994.

Massel, S.R., *Hydrodynamics of Coastal Zones*, Elsevier Science Publishing, Amsterdam 1989.

Mouat, C.T. and R.K. Beatson, *RBF Collocation*, Department of Mathematics and Statistics, University of Canterbury, New Zealand, 2002.

Wertz, J., E.J. Kansa and L. Ling, "The Role of Multiquadric Shape Parameters in Solving Elliptic Partial Differential Equations", *Computers and Mathematics with Applications*, Vol 51, pp. 1335-1348, 2006.

Zhang, X., K.Z. Song, M.W. Lu and X. Liu, "Meshless Methods Based on Collocation with Radial Basis Functions", *Computational Mechanics*, Vol. 26, pp. 333-343, 2000.